

Article

EMBO
reports

Metabolic routing maintains the unique fatty acid composition of phosphoinositides

Yeun Ju Kim¹, Nivedita Sengupta¹, Mira Sohn¹, Amrita Mandal¹, Joshua G Pemberton¹, Uimook Choi² & Tamas Balla^{1,*}

Abstract

Phosphoinositide lipids (PPIn) are enriched in stearic- and arachidonic acids (38:4) but how this enrichment is established and maintained during phospholipase C (PLC) activation is unknown. Here we show that the metabolic fate of newly synthesized phosphatidic acid (PA), the lipid precursor of phosphatidylinositol (PI), is influenced by the fatty acyl-CoA used with preferential routing of the arachidonoyl-enriched species toward PI synthesis. Furthermore, during agonist stimulation the unsaturated forms of PI (4,5P)₂ are replenished significantly faster than the more saturated ones, suggesting a favored recycling of the unsaturated forms of the PLC-generated hydrolytic products. Cytidine diphosphate diacylglycerol synthase 2 (CDS2) but not CDS1 was found to contribute to increased PI resynthesis during PLC activation. Lastly, while the lipid transfer protein, Nir2 is found to contribute to rapid PPIn resynthesis during PLC activation, the faster re-synthesis of the 38:4 species does not depend on Nir2. Therefore, the fatty acid side-chain composition of the lipid precursors used for PI synthesis is an important determinant of their metabolic fates, which also contributes to the maintenance of the unique fatty acid profile of PPIn lipids.

Keywords phosphatidylinositol; phosphatidic acid; diacylglycerol; phospholipase C; lipid transfer proteins

Subject Categories Membranes & Trafficking; Metabolism

DOI 10.1525/embr.202154532 | Received 25 October 2021 | Revised 18 April 2022 | Accepted 4 May 2022 | Published online 16 June 2022

EMBO Reports (2022) 23: e54532

Introduction

Polyphosphoinositides (PPIn) are low-abundance regulatory phospholipids that play crucial regulatory roles in almost all aspects of membrane biology within eukaryotic cells. PPIn lipids were initially found to be central for signal transduction from cell surface receptors that are coupled to phospholipase C (PLC) activation (Michell, 1975; Berridge, 1984). However, it has since been recognized that PPIn lipids have a much wider importance in eukaryotic cells and

regulate virtually every step along the vesicular membrane trafficking continuum as well as directly control the activity of multi-pass transmembrane spanning proteins, such as ion channels and transporters (Balla, 2013; Schink *et al.*, 2016). More recently, some PPIn species were found to control the non-vesicular transport of lipid molecules between diverse membrane compartments and govern many processes linked to the establishment or function of membrane contact sites (Wong *et al.*, 2018; Prinz *et al.*, 2020).

A unique feature of phosphatidylinositol (PI) and its phosphorylated PPIn derivatives is that they are highly enriched in polyunsaturated arachidonic acid at the sn-2 position of the glycerol backbone, such that the sn-1 stearoyl (C18:0); sn-2-arachidonoyl (C20:4) species is the predominant cellular form of PI (Berger & German, 1990; Lee *et al.*, 2012; Anderson *et al.*, 2013; Bone *et al.*, 2017; Traynor-Kaplan *et al.*, 2017). The metabolic processes responsible for regulating this enrichment are not fully understood, nor is it known what importance this unique side-chain composition has for normal cell physiology (Barneda *et al.*, 2019). However, the evolutionary conservation of this unique feature of PPIn lipids, together with their special importance in membrane biology, suggest that this unique and specific fatty acid composition has some significance in relation to the selection of these lipids as ubiquitous regulators of membrane biology (Barneda *et al.*, 2019).

Diversity in the fatty acid side-chain signature is also present in other phospholipids, which highlights the important question of how the various lipid metabolic pathways are spatially organized, and perhaps isolated from one another. This is particularly important considering that specific lipids are directed toward their unique metabolic fates in membranes comprising the endoplasmic reticulum (ER), where almost all cellular lipids are synthesized. Given the fact that phospholipids display a remarkable variety within their fatty acid side-chains, it is tempting to speculate that these unique compositions contain information instructive to their preferred metabolic path or subcellular destination; perhaps functioning as a metabolic barcode. Modern lipidomic analyses using mass-spectrometry now provide an opportunity to investigate this possibility and can also be viewed in combination with complementary methods that can directly assess the dynamics of subcellular lipid

¹ Section on Molecular Signal Transduction, Program for Developmental Neuroscience, NICHHD, National Institutes of Health, Bethesda, MD, USA

² Genetic Immunotherapy Section, Laboratory of Clinical Immunology and Microbiology, NIAID, National Institutes of Health, Bethesda, MD, USA

*Corresponding author. Tel: +1 301 435 5637; E-mail: ballat@mail.nih.gov

distributions in real time or track the metabolic flux through specific lipid synthetic pathways using isotope labeling.

Fatty acid remodeling of phospholipids can be established at the point of their *de novo* synthesis, or as the result of deacylation-reacylation cycles that are also referred to as Lands' cycles (Hill & Lands, 1968). PI is synthesized from phosphatidic acid (PA) by the single phosphatidylinositol synthase enzyme (PIS) via the short-lived intermediate, cytidine-diphosphate diacylglycerol (CDP-DAG) that is produced by two CDP-DAG synthases (CDS1 and CDS2) (Agranoff *et al*, 1958). Indeed, preference for using the stearoyl- and arachidonoyl-enriched forms of PA for conversion into CDP-DAG has been shown *in vitro* for the CDS2 enzyme (D'Souza *et al*, 2014). The critical importance of the Lands' cycle for the unique arachidonate enrichment of PPIn lipids was shown by studies that demonstrated that such enrichment was significantly reduced after inactivation of the Lyso-PI (LPI)-selective acyltransferase, MBOAT7 (Lee *et al*, 2012; Anderson *et al*, 2013). Other acyl-transferases that are also selective for lyso-lipids, such as LPCAT3, which enriches the arachidonoyl content of membranes (although not specifically of PI) and regulates triacylglycerol (TG) sequestration in enterocytes or liver (Hashidate-Yoshida *et al*, 2015), and LYCAT, which promotes the stearoyl-enrichment of PI species in the sn-1 position (Imae *et al*, 2012), may also be involved. However, curiously, silencing of LYCAT changed the total level as well as the 38:4 enrichment of the essential signaling PPIn species PI 4,5-bisphosphate [PI(4,5)P₂], but not of the metabolic precursor PI (Bone *et al*, 2017).

The biggest challenge to maintain the unique fatty acid profile of PPIn lipids occurs during the massive PLC activation that is associated with the stimulation of certain families of cell surface receptors. PLC-mediated hydrolysis of the limited pool of plasma membrane (PM)-localized PI(4,5)P₂ generates substantial amounts of DAG, which is rapidly converted to PA in the PM by DAG kinases (DGKs). Concomitantly, PI synthesis is also increased in the ER and given the limited steady-state level of PI in the PM (Pemberton *et al*, 2020; Zewe *et al*, 2020), PI from the ER is used to support the resynthesis of PI(4,5)P₂ within the PM. Enhanced PI synthesis in the ER utilizes ER-localized PA, only some of which originates from the increased PA levels generated within the PM, the rest being produced by phospholipase D (PLD) or *de novo* synthesized PA (Fig 1A). Increased lipid fluxes through this PLC-triggered accelerated metabolic pathway have been termed the "PI-cycle." This rapid turnover could significantly change the fatty acid profile of PI and its phosphorylated forms; essentially reflecting the composition of the ER-localized PA species that were used for acute PI re-synthesis.

It has been suggested that some of the enzymes that take part in the PI-cycle show preferences towards the stearoyl- and arachidonoyl-containing variants of these lipid intermediates. Namely, DGK ϵ , one of the many isoforms of the mammalian DGKs, shows a preference for the stearoyl–arachidonoyl (38:4) species of DAG *in vitro* (Pettitt & Wakelam, 1999; Epand, 2012), as does CDS2 towards PA (D'Souza *et al*, 2014), while a similar preference is also seen for the type I PIP 5-kinase that generates PI(4,5)P₂ from PI4P (Shulga *et al*, 2012). However, it is still not clear which of the many DGK isoforms are involved in PA generation within the PI cycle. Notably, DGK ϵ is localized to the ER (Nakano *et al*, 2016) and although DGK ϵ knockout mice show decreased levels of PI(4,5)P₂ in the brain and increased resistance to electroconvulsive shock, loss of DGK ϵ does not appear to generally disrupt PLC-triggered

signaling (Rodriguez de Turco *et al*, 2001). In addition to the synthetic machineries, selection of phospholipids specifically bearing the 38:4 fatty acid signature could also occur during the non-vesicular transport processes that facilitate the transfer of lipids between the organelle membranes, including at the ER-PM contact sites. Lipid transfer proteins may actually be more suitable for showing preferences for specific side-chain-containing variants of lipids as they make extensive contacts with the fatty acid backbones of their preferred lipid cargoes. These structural features place lipid transfer proteins as possible molecular devices that could direct unique phospholipids or other metabolites toward specific metabolic pathways.

The first step to finding out the significance of the unique fatty acid signature of PPIn lipids is to understand the mechanism that is responsible for the establishment and maintenance of this unique enrichment. Although numerous studies have previously provided important information about these questions, the fact that they used a variety of different cell types and only addressed a subset of these important questions makes it difficult to establish a coherent picture regarding these complex metabolic pathways. The goal of the present study was to investigate the metabolic isolation or intermixing of the PA pools originating from different metabolic pathways such as *de novo* synthesis or PLC- and PLD-mediated PA generation, as well as trace their utilization for PI synthesis. We present data obtained using a combination of approaches, all applied to a single cell line, to gain comprehensive information on the metabolic fates of PI precursors by following their side-chain signature and matching their kinetics with BRET-based lipid measurements specifically within the PM. Lipidomics analyses were combined with isotope labeling and pharmacological studies to identify differences in the handling of lipid intermediates with a specific fatty acid composition that are involved in PPIn homeostasis. These studies suggest that metabolic routing of PA occurs at the ER and shows a clear preference for the DAG and PA that originated from PI(4,5)P₂ breakdown for conversion to PI and ultimately back into PI(4,5)P₂ upon PLC activation.

Results

The steady-state fatty acid compositions of PI and its metabolic precursors show major differences

Fig 1A and B show simplified schematics of the known metabolic compartmentalization of PPIn biosynthesis and turnover, the subject of the current study. All experiments were performed using HEK293-AT1 cells, a HEK293 clone stably expressing the rat AT1 angiotensin receptors (Hunyady *et al*, 2002), which were subjected to lipidomics analyses without any inhibitor treatment or stimulation. Without compartmentalization or active metabolic channeling, it is expected that the fatty acid composition of the phospholipid classes will be unchanged and reflect a simple substrate-product relationship. However, as has been well documented in the literature (Possmayer *et al*, 1969; Holub & Kuksis, 1971b; Lee *et al*, 2012; Anderson *et al*, 2013), all five major phospholipid species (PA, PI, PC, PE and PS) and DAG, display significant differences in their fatty acid side-chain compositions (Fig 1C). The dominant PI species was the 38:4 (stearoyl–arachidonoyl) variety, although significant

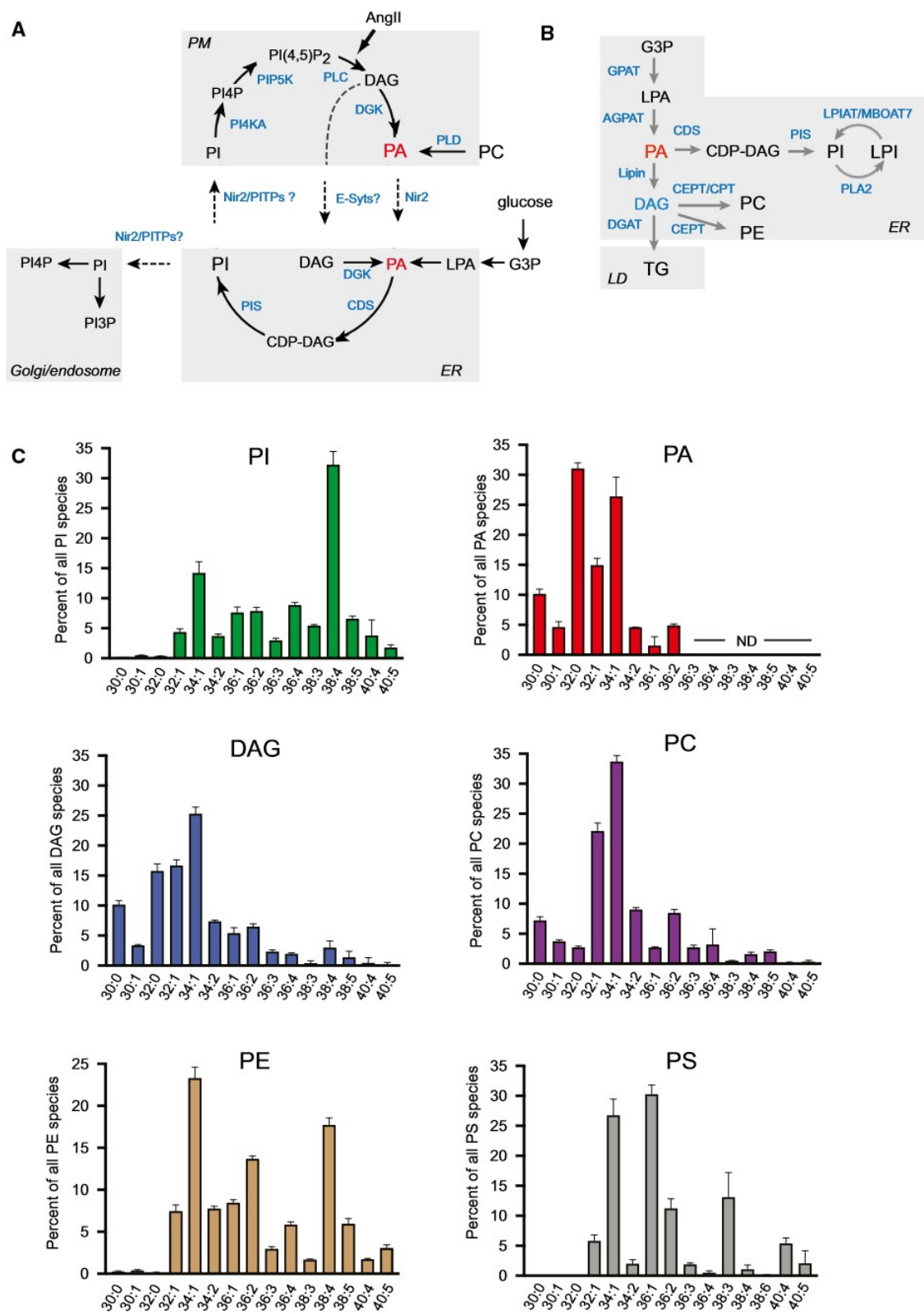


Figure 1.

Figure 1. Metabolic pathways used for phospholipid synthesis and phosphatidylinositol turnover in a mammalian cell and the fatty acyl side-chain profile of phospholipids in HEK293-AT1 cells.

- A Receptor-induced hydrolysis of phosphatidylinositol (PI) 4,5-bisphosphate (PI(4,5)P₂) by phospholipase C (PLC) leads to the direct formation of diacylglycerol (DAG), which is rapidly converted to phosphatidic acid (PA) within the plasma membrane (PM). PA can be transferred to the endoplasmic reticulum (ER) where it is used to resynthesize PI, via a CDP-DAG intermediate. Transfer of PI into the PM is essential for the maintenance of the PM pool of PI(4,5)P₂. While the multi-domain PI-transfer protein Nir2 has been shown to play a role in non-vesicular PA and PI transport between the PM and the ER, it is not clear if there are additional lipid transfer mechanisms that are also involved in the inter-organelle transport of these lipids. It is also unclear whether the ability of extended synaptotagmins (E-Syts) to control the transfer of DAG from the PM to the ER under high Ca²⁺ conditions also contributes to lipid redistribution during receptor activation. Notably, PI also serves as a precursor for PI 3-phosphate (PIP3) and PI 4-phosphate (PIP4P) in endosomal membranes, as well as at the Golgi complex, but it is not known what lipid transfer mechanisms play a role in supplying PI from the ER to these membranes for PPI production.
- B Enzymatic steps in the *de novo* synthesis of phospholipids from glycerol-3-phosphate (G3P). Several genes encode enzymes, called GPATs, that esterify the *sn*-1 position of G3P using fatty acyl-CoA to produce lyso-PA (LPA), whereas the enzymes that catalyze the conversion of LPA to PA, are called AGPATs. *De novo* synthesized PA serves as an important metabolic hub, which can be used directly for PI synthesis or alternatively used for phospholipid or triglyceride (TG) synthesis after dephosphorylation to DAG by the Lipin family of phosphatases. Remodeling of the fatty acid side chains on phospholipids can take place through deacylation-reacylation cycles, called Land's cycles, such as the one depicted here for PI.
- C Results from lipidomics analyses of HEK293-AT1 cells are shown, with each fatty acid side-chain variant represented as a percentage of the total pool of the indicated lipid class. Average values (\pm SEM) were calculated from three independent analyses, each performed on three separate culture dishes that served as triplicates. Note the striking discrepancy between the side-chain signatures of PI and its immediate metabolic precursor, PA; which has also been documented in previous studies (Possmayer *et al.*, 1969; Holub & Kuksis, 1971b; Anderson *et al.*, 2013). ND: not detected.

amounts of other forms were also present, including most prominently the 34:1 variant (Fig 1C). This side-chain distribution was consistent with earlier findings showing that cultured cells possess a greater variety of PI species when compared to native tissues, which have an even more pronounced enrichment in the 38:4 variant. The relative representation of different PI species can also depend on the cell culture conditions used (Anderson *et al.*, 2016; Traynor-Kaplan *et al.*, 2017). This heterogeneity proved to be useful for the present study as it allowed us to trace the source and turnover of the specific metabolites generated from these major pools of PI species. Importantly, in unstimulated cells, the dominant PA species were the short-chain saturated variants, namely 30:0, 32:0, and 34:0, as well as the monounsaturated 34:1 form. Notable was the lack of the 38:4 species under these basal conditions (Fig 1C). DAG showed a broader fatty acid side-chain distribution, but the shorter acyl chain-containing forms were still more abundant. Although in a relatively small amount, the presence of 38:4 species was detected among the DAG variants (Fig 1C). The dominant PC species were the 32:1 and 34:1 forms; longer and more unsaturated variants were also present although in smaller amounts (Fig 1C). PE and PS showed unique and dissimilar fatty acid profiles that were markedly different from one another and also different from those observed for DAG and PC (Fig 1C). The striking difference between the fatty acid side-chain profiles of PA and PI suggested that conversion of PA to PI is not indiscriminate and, as shown by previous studies (Lee *et al.*, 2012; Anderson *et al.*, 2013), PI undergoes significant side-chain remodeling, likely mediated by the LPIAT1/MBOAT7 enzyme, after it is synthesized (Fig 1B).

The metabolic fate of *de novo* synthesized PA is influenced by its fatty acid side-chain composition

Since PA is generated from various lipid sources within the ER, each yielding a different fatty acyl-chain composition, we set out to investigate whether the metabolic fate of ER-localized *de novo* synthesized PA differs depending on its side-chain profile. For this, we followed the metabolism of *de novo* synthesized PA using microsomes prepared from HEK293-AT1 cells and employed ¹⁴C-labeled glycerol 3-phosphate (G3P) together with different fatty acid-CoA

analogues as substrates. Radioactive products were separated by thin-layer chromatography (TLC) (Fig 2A–C). When palmitoyl-CoA was used along with ¹⁴C-G3P, the majority of the radioactivity was found in PA and TG without significant activity associated with LPA (Fig 2A). When cytidine triphosphate (CTP) was added, labeling appeared in CDP-DAG as well as PC, and only upon further addition of *myo*-inositol did labeling of PI appear (Fig 2A). Interestingly, the inclusion of R59022, a broad-spectrum inhibitor of DGKs (DGKi), in the assay reduced the PI signal and slightly increased the amount of TG (Fig 2A). These data suggested that at least some of the PI must have been generated indirectly from *de novo* synthesized PA through a conversion to DAG and subsequent re-phosphorylation by a resident DGK enzyme; a reaction that appears to occur even without the addition of exogenous ATP. When microsomes were prepared from cells expressing the PA-selective phosphatase, Lipin1γ, substantially more TG was produced (Fig 2B). Notably, there were no increases in DAG observed under these conditions and the addition of CTP or CTP + *myo*-inositol, still generated PC and PI, respectively, as well as significantly diverted PA away from forming TG in both cases. These results suggest that *de novo* synthesized PA is efficiently used for TG synthesis, and that all enzymatic components were functional in this microsomal membrane preparation.

After establishing the utility of this approach, we set out to compare the fate of various fatty acyl-CoA analogues in this *in vitro* membrane preparation. We found major differences between the metabolic incorporation of these analogues. First, oleoyl-CoA showed the largest fractional conversion to TG (Fig 2C and E) in agreement with the well-documented ability of oleic acid to stimulate the formation of lipid droplets (Walther *et al.*, 2017). The second highest conversion efficiency of PA into TG was observed using arachidonoyl-CoA, even though this analogue showed relatively poor incorporation into PA, while stearoyl-CoA showed very little conversion into any of the lipid products (Fig 2C and E). When CTP and *myo*-inositol were added, we observed labeling of PI as well as a slight reduction in the signal associated with TG, suggesting that PA was diverted towards PI synthesis and away from TG production. Similarly, addition of CDP-choline strongly inhibited the conversion of PA into DAG or TG and, instead, increased the signal

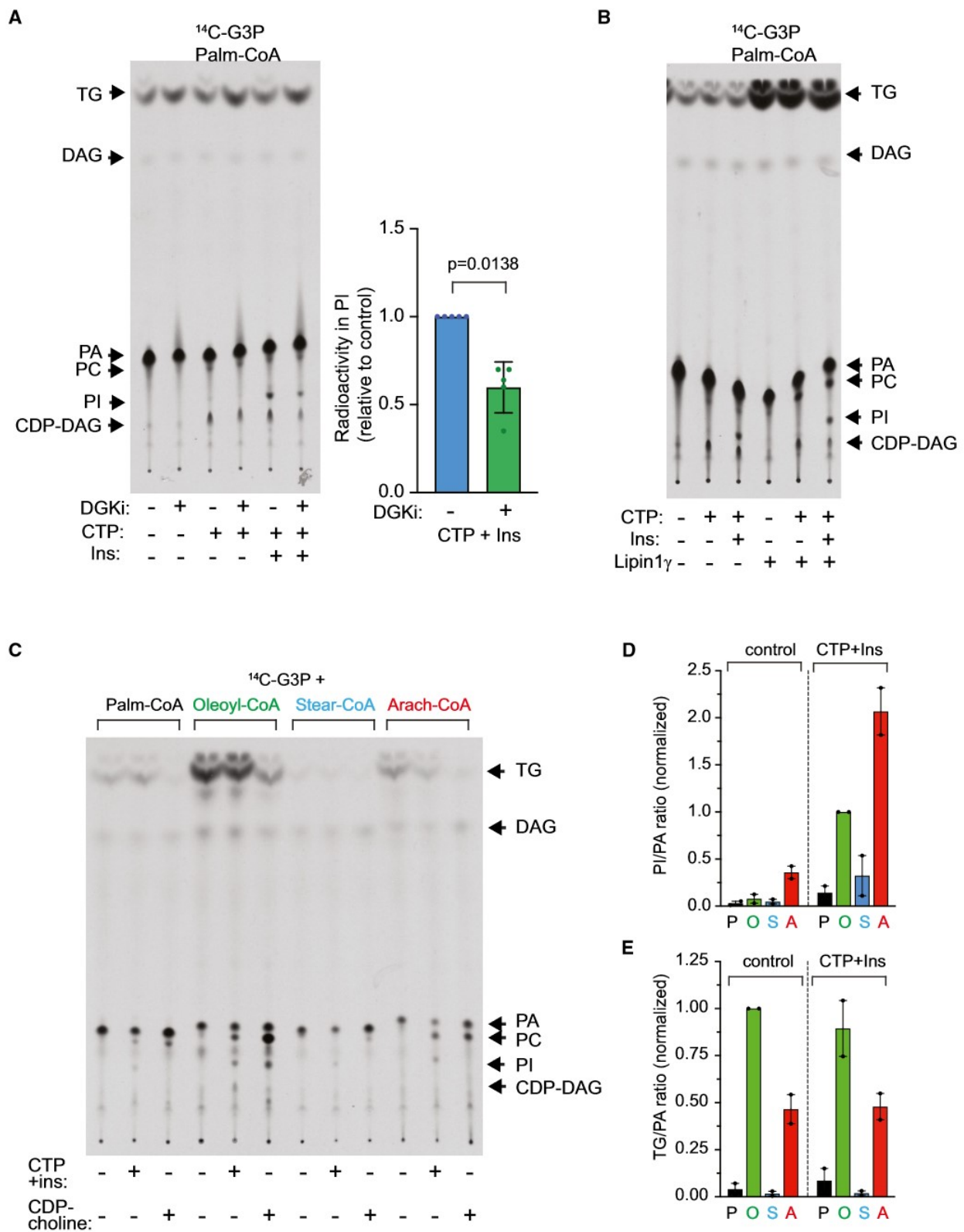


Figure 2.

Figure 2. Metabolic fate of *de novo* synthesized phosphatidic acid using different fatty acid substrates in microsomal membrane preparations.

- A Incorporation of ^{14}C -labeled glycerol 3-phosphate (G3P) into various lipids in the presence of palmitoyl-CoA (10 μM) in microsomal membranes prepared from HEK293-AT1 cells. After incubations at room temperature for 30 min, lipids were extracted and separated by TLC before quantification using autoradiography and phosphorimaging. For more experimental details, refer to the Materials and Methods. Lipid species corresponding to the major spots visualized are indicated. Note the appearance of phosphatidylcholine (PC) and cytidine diphosphate-diacylglycerol (CDP-DAG) in the presence of cytidine triphosphate (CTP), as well as the production of phosphatidylinositol (PI) only when both CTP and *myo*-inositol are present. Also, there is a relatively small effect of the DAG kinase inhibitor (DGKI) on CDP-DAG and PI formation in spite of the fact that plenty of phosphatidic acid (PA) is available from *de novo* synthesis (although it should be noted that no ATP was added during these reactions). A representative experiment is shown, but these results have been reproduced in other replicates using different treatment combinations. The insert shows the effect of the DGKI inhibitor on PI labeling (mean \pm SD, $n = 5$ biological replicates).
- B Effect of *lipin1y* overexpression on the metabolic fate of *de novo* synthesized PA. Experiments were performed as in panel A, except that the membranes were also prepared from cells expressing a GFP-tagged *lipin1y*, as indicated. Note the large amount of TG and increased production of PC under these conditions. Results of a representative experiment are shown, and these experiments were repeated with identical results.
- C-E Effect of different fatty-acyl-CoA analogs (each used in 10 μM) on the metabolic fate of *de novo* synthesized PA. Note the preferential conversion of oleoyl-CoA containing PA into TG and the very poor incorporation of stearoyl-CoA into TG. Arachidonoyl-CoA is a relatively poor substrate for the generation of *de novo* synthesized PA; however, this substrate has the highest conversion rate into PI, which was calculated as the ratio of the PI and PA radioactivity shown in panel D. A representative autoradiogram is shown in (C), while quantified values (means \pm range) from two such experiments are shown in (D) and (E).

associated with PC (Fig 2C). There was also a strong signal migrating with PI in the CDP-choline treated sample, but only in the oleoyl-CoA treated group. This was attributed to the increase in the inositol base-exchange reaction between the endogenous PI and the radioactive PA, which can be facilitated by cytidine monophosphate (CMP) liberated from CDP-choline, as described in early studies (Agranoff *et al.*, 1958; Holub, 1975). This interesting observation, however, was not further pursued in the present study.

Since the different fatty acid analogues were not used equally to generate PA, we calculated PI/PA and TG/PA incorporation ratios from these experiments in order to estimate the relative conversion of these fatty acid analogues beyond the PA labeling step. These ratios showed that the highest conversion of PA into PI resulted from the exogenous supply of arachidonoyl-CoA, whereas the oleoyl-CoA showed the best conversion into TG (Fig 2D and E). Saturated fatty-acid analogues of PA were poorly converted to both phospholipids and TG. Overall, these studies allowed us to make the following conclusions: first, unsaturated fatty acids are the preferred substrates for incorporation into both phospholipids and TG during *de novo* PA synthesis. Second, among the saturated fatty acids, the shorter palmitoyl species can still be efficiently incorporated into PA, while stearoyl-CoA is poorly used during *de novo* synthesis, which suggests that its incorporation into phospholipids occurs primarily in deacylation–reacylation cycles, perhaps mediated by the LYCAT enzyme (Imae *et al.*, 2012). Third, some selection for the arachidonoyl enrichment occurs during the synthesis of PI, most likely at the step of CDP-DAG production. This latter observation is consistent with reports showing that the CDS enzymes (Saito *et al.*, 1997; D'Souza *et al.*, 2014), but not PIS (D'Souza & Epand, 2015), exhibit preference for stearoyl- and arachidonoyl-acylated precursors using *in vitro* assays.

However, it should be noted that the addition of a single acyl-CoA species during these assays does not effectively mimic the *in vivo* situation, where a mix of the various fatty acids are present in some dynamic proportion. We have therefore tested whether a combination of fatty-acyl-CoA species could significantly alter the relative incorporation measurements made using this assay. These experiments, however, did not indicate any specific interactions between the various acyl-CoA species and simply reflected the sum of what was already observed using the individual acyl-CoAs (Fig EV1). Simply stated, unsaturated acyl chains were clearly the preferred substrates, especially at longer chain lengths.

The fatty acid signature of DAG suggests that DAG is rapidly converted to PA in the PM during receptor-mediated PLC activation

So far, we have studied the source of the arachidonoyl enrichment observed in PI during its synthesis from the *de novo* pathway that occurs within the ER. Next, we turned our attention to the lipid products generated during stimulation of cells with a PLC-coupled agonist, angiotensin II (AngII), which selectively triggers the hydrolysis of the PM pool of PI(4,5)P₂. Treatment of cells with AngII (100 nM) for 10 min caused notable changes in the fatty acid profile observed for the various phospholipids, including clear alterations to the PI, DAG, and PA species observed. Notably, there was no change in any of the PC species (Fig 3A), whereas almost all PI species showed a small decrease of ~20% (Fig 3A). Increases in DAG were moderate at the 10 min time point, especially in the 38:4 form, while the bulk of the increases were detected in the shorter variants, mostly in the 32:1 and 34:1 species (Fig 3A). The small increase in the 38:4 form of DAG was consistent with its rapid conversion to PA in the PM. To test this possibility, we performed additional experiments to monitor the DAG levels at earlier time points following stimulation, specifically in the PM. First, we used bioluminescence resonance energy transfer (BRET) measurements to follow the DAG changes in the PM after AngII stimulation using the tandem C1 domains from protein kinase D (PKD-C1ab) as a DAG reporter (Pemberton *et al.*, 2020). Briefly, these BRET measurements reflect the molecular proximity between an organelle-targeted mVenus protein, in this case localized to the PM, and a luciferase enzyme fused to the lipid-sensing domain of interest (Toth *et al.*, 2019). Although this approach does not discriminate between the various fatty acid variants of DAG, it does monitor the PM-specific changes in DAG levels as they originate from PI(4,5)P₂ hydrolysis. These studies showed a rapid and transient increase in DAG levels within the PM that was followed by a lower, but still elevated plateau phase (Fig 3B). Lipidomic analyses of the DAG content covering this early period also showed a biphasic increase in the total DAG mass, with an early peak and a slower sustained increase (Fig 3C). Although the magnitude of the observed changes in the 38:4 DAG species differed between the two lipidomic experiments, both showed only a transient elevation, which is in agreement with the kinetics observed in the BRET measurements (Fig 3D). In contrast, the dominant 34:1 form showed a smaller and more steady

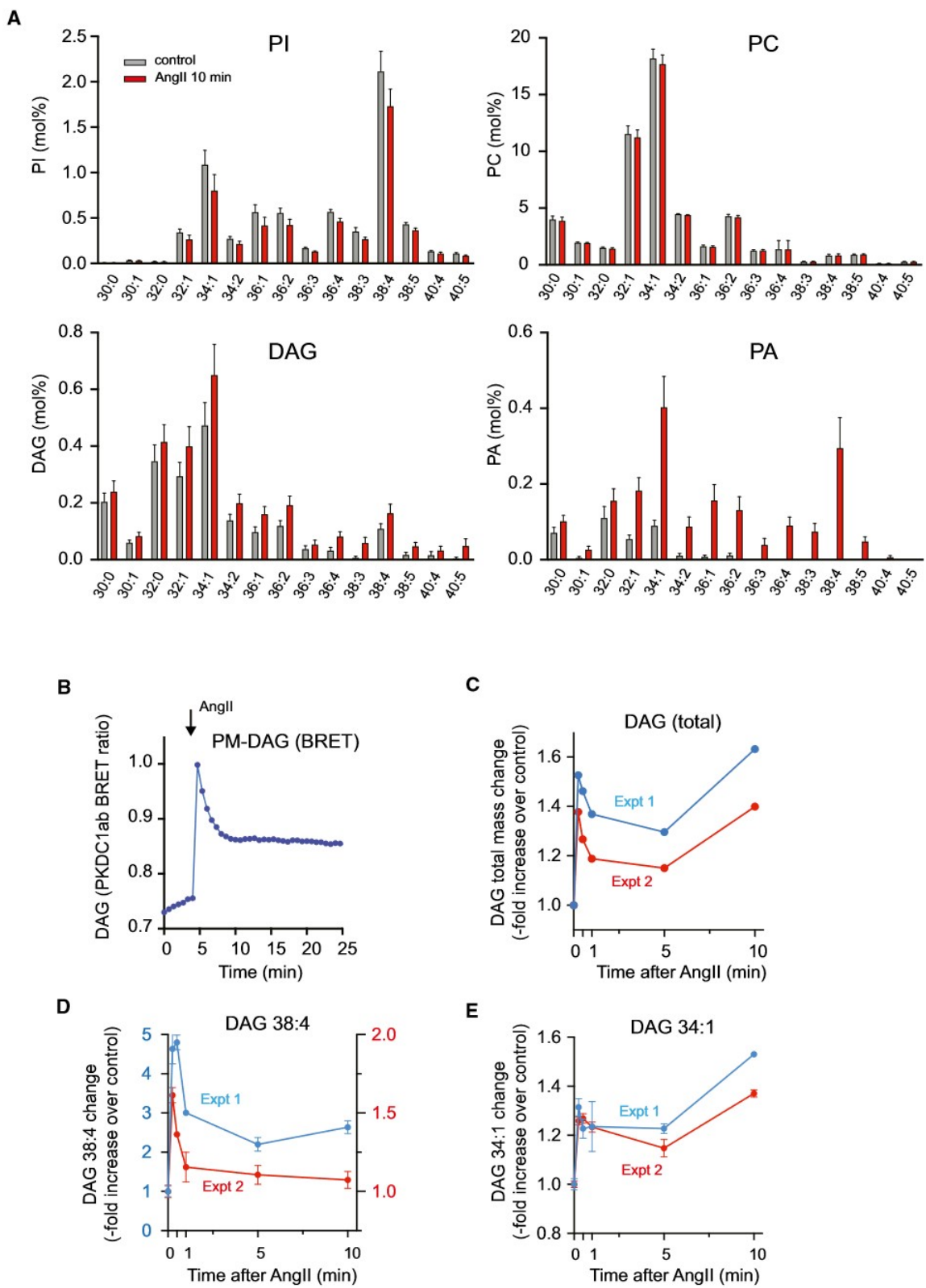


Figure 3.

Figure 3. Effects of angiotensin II (AngII) stimulation on the relative levels of diacylglycerol and other phospholipid variants.

- A Lipidomics analyses were performed using HEK293-AT1 cells before (grey columns) and after stimulation of the cells with AngII (100 nM) for 10 min (red columns). Mean \pm SD of the normalized mol% values within each lipid class were calculated from four independent experiments, where three separate culture dishes served as internal triplicates. Note the small, but consistent decrease in most of the highly represented phosphatidylinositol (PI) species, as well as the large increases in many phosphatidic acid (PA) species; some of which were not detected without stimulation. Only small increases were observed for diacylglycerol (DAG) species, whereas no major changes in phosphatidylcholine (PC) forms were observed.
- B Bioluminescence resonance energy transfer (BRET) measurements of DAG levels within the plasma membrane (PM) after stimulation of HEK293-AT1 cells with AngII using the C1ab domains of protein kinase D as a DAG reporter. Note the transient nature of the DAG increase, which is caused, in part, by the rapid conversion of DAG into PA and also as the result of the desensitization of the AT1 receptors (means \pm SEM of triplicate measurements; note that the error bars are smaller than the symbols).
- C Time course of total DAG changes after AngII stimulation as assessed by lipidomic analyses from two independent experiments performed in triplicate. Fold increases in DAG levels over the unstimulated controls were calculated from the mol% values and the results of two independent experiments are shown in different colors.
- D, E Time course studies specifically showing the relative amounts of the 38:4 and 34:1 DAG species, as measured from two different lipidomic analyses (means \pm SEM of biological triplicates). Note the different scales along the Y-axes for the two experiments in panel D.

increase (Fig 3E). These results suggest that the early increases in the 38:4 and 34:1 species of DAG reflect their rapid formation from PI(4,5)P₂ in the PM through PLC activation, which is followed by a subsequent conversion to PA. However, additional processes, such as *de novo* synthesis could contribute to the slower increase in DAG species with shorter and more saturated side chains, including some of the 34:1 species.

The fatty acid signature of PA products during agonist stimulation reflects primarily PLC activation and only minor roles for PLD activity or *de novo* PA synthesis

The largest changes in the lipid profile after 10 min AngII stimulation were observed in PA. First, many more PA variants appeared after stimulation with AngII, including many species that were not detected in unstimulated cells, such as the 38:4 form. Some of these variants clearly matched the fatty acid profile of PI as well as PIP₂ (see below), and hence were the result of PLC activation. Importantly, however, there were also increases in PA species that were not represented in PI, such as the 30:0, 30:1, and 32:0 forms (Fig 3A), which makes them unlikely to be the products of direct PLC-generated hydrolysis of PI(4,5)P₂. To determine the relative contribution of potential enzymatic pathways contributing to the AngII-induced PA increases, we first examined the contribution of phospholipase D (PLD) activity. Cells were stimulated with AngII for 10 and 20 min in the absence or presence of 1 μ M of the selective pan-PLD inhibitor, F1PI, and then subjected to lipidomics analyses. F1PI treatment caused a minor inhibition of PA production that was almost exclusively detected in the 32:1, 34:1, and 34:2 species (Fig 4A, grey boxes). This side-chain profile matched the general fatty acid profile of PC (see Figs 1C and 3A). Notably, there was no effect of F1PI on the amount of PA possessing the 38:4 fatty acid signature (Fig 4A, blue box). These data suggest that PLD activity was only a minor contributor toward PA generation downstream of AngII stimulation.

We then investigated the effects of DGK inhibition on PA generation during AngII stimulation. Again, the cells were stimulated with AngII for 10 and 20 min with or without a 10-min preincubation with R59022 (DGKi; 50 μ M). This experiment showed that the AngII-induced increase in almost all of the various PA species was reduced, but not completely abolished, by DGK inhibition (Fig 4B). To better assess the extent of the DAG to PA conversion, we calculated the ratio of PA/DAG for each of the major side-chain variants (Fig EV2A). Overall, these data raise the possibility that some of the

many isoforms of DGKs are not fully inhibited by R59022 (Sato *et al*, 2013). However, since the PLC-generated DAG requires a PM-localized DGK to be converted to PA, it is not surprising that the AngII-induced increases in the 38:4 and 34:1 forms of PA were reduced by treatment with DGKi. It is less clear whether the AngII-induced elevations in the shorter and saturated PA variants reflect the actions of DGKs present in other membrane compartments and/or on DAG sources not directly generated by PI(4,5)P₂ hydrolysis within the PM.

One of the limitations of these lipidomics studies is that they provide no information about the subcellular distribution of the various PA species. To evaluate the PA changes specifically within the PM, and the relative contribution of PLD and PLC to these changes, we performed BRET analysis using the Spo20-based PA sensor (Kim *et al*, 2015) to detect the PA levels in the PM after AngII stimulation. We have established this approach for the specific detection of PA at the PM using cell population-level measurements (Gulyas *et al*, 2020; Pemberton *et al*, 2020). These experiments showed a slow but prominent accumulation of PA at the PM after AngII stimulation that was only marginally reduced by pretreatment with F1PI and strongly, although not completely, inhibited by 5 μ M of the putative PLC inhibitor, U73122 (5 μ M; Fig 4C-E). Similar BRET measurements showed that DGK inhibition substantially decreased basal PA levels within the PM, as well as reduced the increase in PA in this compartment after AngII stimulation, but, again, did not completely eliminate this response (Fig 4D). These findings were consistent with the results of our lipidomics data.

Collectively, these studies support the conclusion that AngII stimulation of PLC rapidly generates DAG within the PM, and that PLD does not significantly contribute to the increase in the 38:4 form of PA. Several other PA species also show prominent increases after AngII stimulation and, for the most part, they reflect the acyl-chain composition of PI and PI(4,5)P₂; except for the short and saturated forms that likely reflect an increase in *de novo* synthesis. The minimal contribution of PLDs to PA generation is restricted to the 32:1 and 34:1 chain variants matching the resting fatty acyl profile of PC.

Radioisotope labeling of lipids shows that increased PI synthesis during agonist-induced PLC activation preferentially uses PLC-generated DAG and PA

It is well-documented that PLC activation increases PI synthesis, which is reflected in the increased incorporation of ³²P-phosphate or myo-[³H]-inositol into PI within intact cells (Michell, 1975). It has

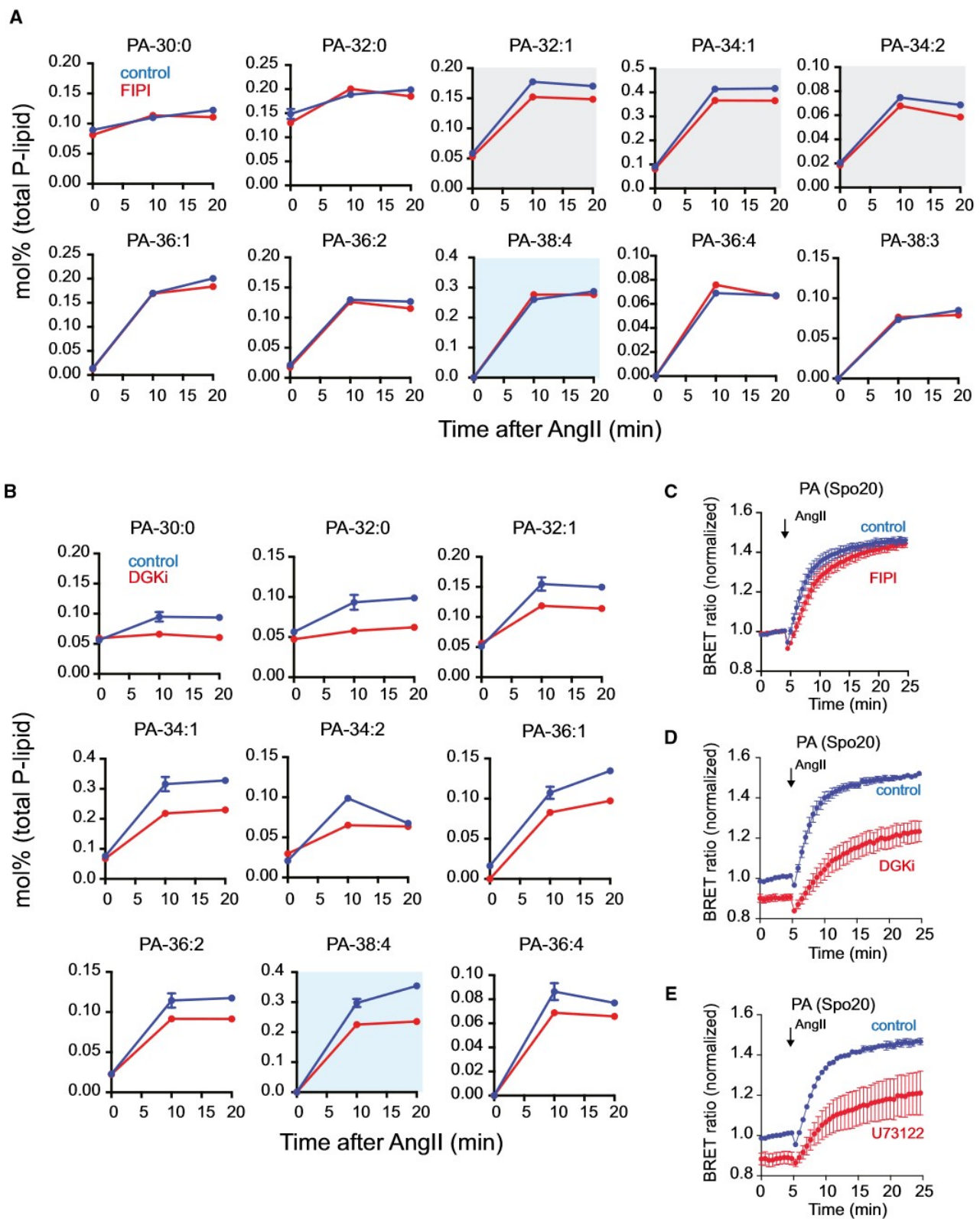


Figure 4.

Figure 4. Pharmacological assessment of the metabolic turnover of phosphatidic acid species following AngII-stimulation.

- A HEK293-AT1 cells were stimulated with AngII for 0, 10, or 20 min in the presence or absence of the selective phospholipase D (PLD) inhibitor FIP1 (1 μ M). Cells were preincubated with FIP1 or a DMSO vehicle control for 10 min before the addition of AngII (100 nM). After treatments, cells were harvested and subjected to lipidomics analyses. Changes in the various species of phosphatidic acid (PA) are shown as a mol% of total lipids (means \pm SEM from an experiment performed using triplicate wells). Some error bars are smaller than the symbols. Of all the PA species that increase upon AngII stimulation, only three show a small inhibition after pretreatment with FIP1 (32:1; 34:1, and 34:2, highlighted in gray). These species directly correspond to the fatty acid profile of the major cellular pools of phosphatidylcholine (PC; see Fig 2D or Fig 4B). There was no effect of FIP1 on the increase observed in the 38:4 PA species that is derived from the major species of PI (4,5)P₂ (highlighted in light blue). Please note the differences in the scale of the Y-axes; these differences reflect the unique representation of the various PA forms in cells, with some species below the level of detection in unstimulated samples.
- B Identical experiments to those performed in (A) were repeated instead using a diacylglycerol kinase (DGK) inhibitor, R59022 (DGKi; 50 μ M). The increase observed in almost all PA species in response to treatment with AngII was reduced by pre-treatment with DGKi, but not completely eliminated (mean \pm SEM, $n = 3$ biological replicates).
- C-E Bioluminescence resonance energy transfer (BRET) measurements of the changes in PA levels within the plasma membrane (PM) of HEK293-AT1 using a modified Spo20-based PA sensor. Responses were measured in cells following AngII stimulation alone or in combinatorial treatments with either FIP1 (C), DGKi (D), or 5 μ M U73122 (E). BRET ratios were normalized to the pre-stimulatory values of DMSO-treated cells. Means \pm SEM are shown from three experiments performed in triplicate wells. Note the minor inhibitory effect of FIP1, which is consistent with the lipidomics results. PA basal values are also greatly reduced in the PM following pre-treatment with the DGKi, or U73122, but the increases are not completely eliminated. The minor drop in the signal right after stimulation reflects the anionic PI (4,5)P₂ decrease since this sensor can also bind to PI(4,5)P₂ to a small extent.

been the accepted view that this increase is the result of the enhanced production of inositol 1,4,5-trisphosphate (Ins(1,4,5)P₃) and DAG from PI(4,5)P₂ with subsequent conversion of DAG into PA within the PM and its subsequent transport to the ER (see (Chang & Liou, 2016) for a recent review). To revisit the question whether PLC-mediated generation of DAG was the sole reason for increased PI synthesis during agonist stimulation, we performed radioisotope experiments using HEK293-AT1 cells in combination with selective inhibitors targeting the various sources of PA production (Fig 5A). Relatively short-term labeling with radioactive precursors provides information on the rate of synthesis rather than changes in the size of the lipid pool in question and therefore can complement the lipidomic analyses that report on absolute levels of the lipids. As shown in Fig 5B, AngII stimulation enhances the short-term (1h) incorporation of [³H]-inositol into PI. This increase was only partially inhibited by the PLC inhibitor, U73122, but was completely eliminated by treatment with DGKi. Importantly, inhibition of PLD by FIP1 had only a minor effect on [³H]-inositol incorporation (Fig 5B). However, it is important to note that [³H]-inositol incorporation into PI is not necessarily a true indicator of PI synthetic rate due to the inositol-exchange activity of the PIS enzyme (Koreh & Monaco, 1986; Lykidis *et al.*, 1997). Therefore, we analyzed the effects of the various inhibitors on CDP-DAG production using [³H]cytidine labeling following inositol deprivation combined with Li⁺ treatment. This experimental setup limits CDP-DAG conversion to PI and allows for the detection of CDP-DAG in our cells. Results from these studies show that the AngII-induced CDP-DAG increase was variably inhibited by U73122 treatment and completely abolished by the DGKi, while FIP1 was without significant effect (Fig 5C). As an important control, we determined that the DGKi used did not directly inhibit the PIS or the CDS enzymes using crude membrane preparations (Fig EV2B and C).

Next, given the established importance of the PA conversion to CDP-DAG, we evaluated the relative importance of the two CDS enzymes for the observed increase in PI resynthesis during PLC activation using knock-down experiments. Notably, in these studies, we also included genetic manipulations of the DGKe enzyme, since it has been found to show a preference for the 38:4 fatty acyl configuration (Pettitt & Wakelam, 1999; Epand, 2012). Measurements using both [³H]-cytidine and [³H]-inositol labeling were performed in

unstimulated cells and after treatment with AngII. The efficiency of the siRNA-mediated gene knock-down was assessed by qPCR (Fig EV3A). As shown in Fig 5D, knock-down of CDS2, but not CDS1 or DGKe, significantly inhibited the CDP-DAG response to AngII stimulation. Importantly, relative to the knock-down of CDS2 alone, the combined knock-down of both CDS enzymes did not cause further inhibition of the CDP-DAG labeling. The effects of the various genetic manipulations on [³H]-inositol labeling were essentially the same, except for the relative degree of the inhibition being smaller, which is consistent with the inositol exchange reaction masking some of the effects (Fig 5E).

Taken together, these experiments allowed us to draw the following conclusions: first, agonist stimulation increases PI synthesis, and this increase correlates with PLC activity based on the similar, although partial, inhibitory effect of U73122 on CDP-DAG production and PA generation in the PM. Second, activation of PLD has minor contributions to the increased CDP-DAG synthesis, while the enhanced [³H]-inositol incorporation into PI either reflects an increase in inositol exchange activity or PI synthesis, which also shows close correlation with the observed increases in PA. Third, CDS2 and not CDS1 plays a role in the increased resynthesis of PI during agonist-stimulated PLC activation. Lastly, the strong inhibitory effect of the DGKi on all of the PI synthetic intermediates indicates that recycling the products of PLC activity must originate through phosphorylation of DAG using primarily DG kinase(s) that are sensitive to R59022 and DGKe does not appear to play an important role in this process.

Fatty acid composition determines the recycling efficiency of PI (4,5)P₂ hydrolytic products during PLC activation

AngII stimulation of HEK293-AT1 cells evokes a rapid decrease in the bulk PM levels of PI(4,5)P₂ with a slow and partial recovery (Balla *et al.*, 2007; Kim *et al.*, 2015; Sohn *et al.*, 2018). To analyze the PI(4,5)P₂ changes during AngII stimulation, including information on the various fatty acid side-chain species, a time-course of absolute PIP₂ levels was measured by lipidomics. Although these analyses do not distinguish between the various stereoisomers of PIP₂, given the lower abundance of PI(3,4)P₂ and PI(3,5)P₂, relative to PI (4,5)P₂ (Hasegawa *et al.*, 2017; Malek *et al.*, 2017; Morioka *et al.*,

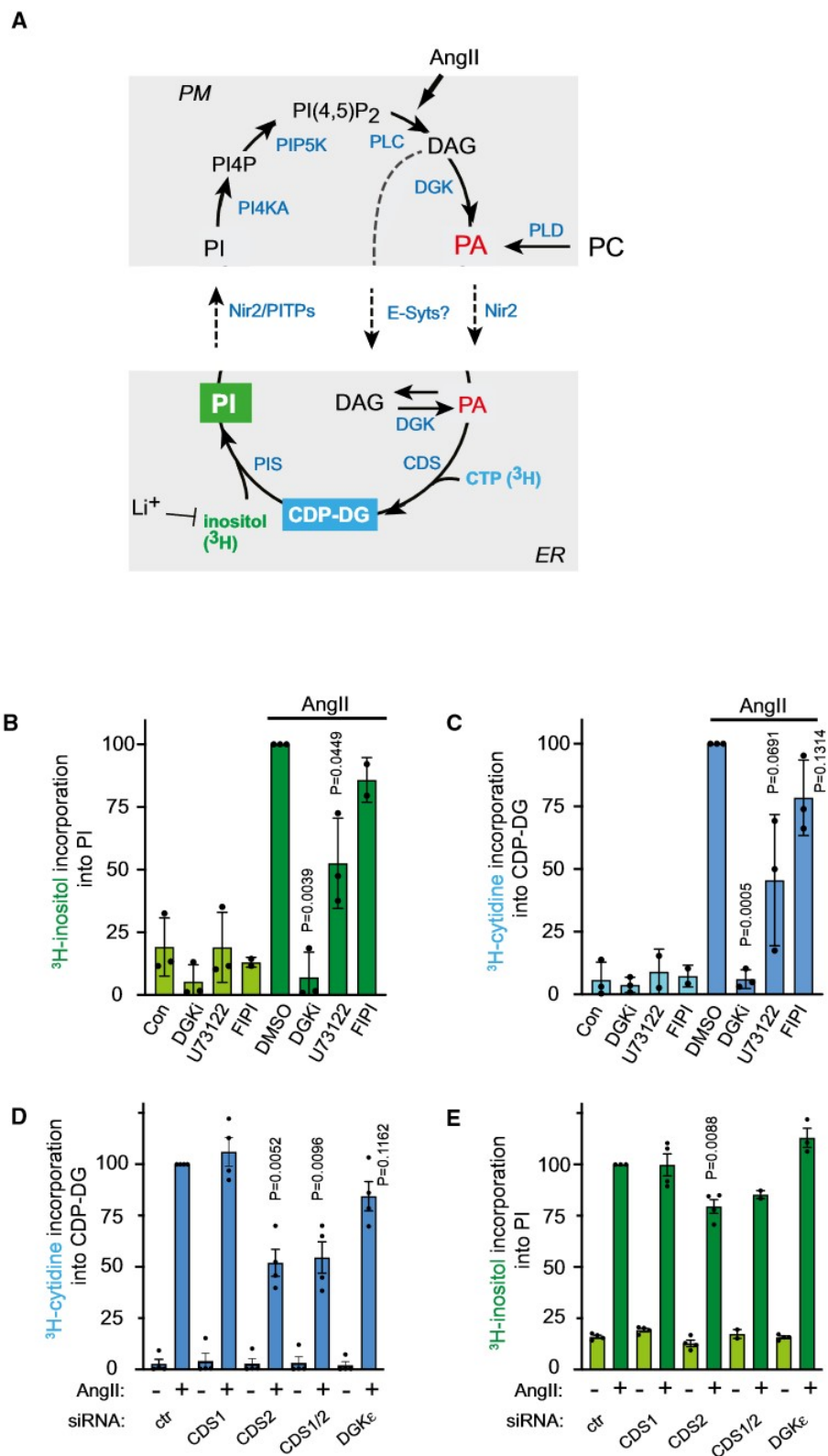


Figure 5.

Figure 5. Isotope labeling of PI cycle intermediates in HEK293-AT1 cells and their response to AngII stimulation.

- A Schematic of the sequential metabolic activities that comprise the "PI-Cycle." The enzymatic steps where the isotope incorporation occurs with the various labeling methods are indicated.
- B Myo-[³H]-inositol incorporation into phosphatidylinositol (PI) occurs at the enzymatic step catalyzed by PI synthase (PIS). This enzyme also has an inositol exchange activity that makes it more difficult to assess whether increased [³H]-labeling reflects new PI synthesis or increased exchange activity. AngII stimulation substantially increases the labeling of PI over a 60-min incubation period (dark green) and this response is completely eliminated by DGK inhibition (R59022, 50 μM) and partially inhibited by treatment with the phospholipase C (PLC) inhibitor U73122 (5 μM), while treatment with a phospholipase D inhibitor (FIP1; 1 μM) had only a slight effect. Note that DGKi already impaired the basal inositol labeling. Values (mean ± SEM) of duplicate measurements from three independent experiments are shown, except for the FIP1 groups that were only repeated twice. Notably, the effects of U73122 showed significant batch-to-batch variations and this was true for all experiments where this inhibitor was used.
- C [³H]-cytidine labeling of CDP-DAG was performed in inositol-free medium and in the presence of Li⁺ (10 mM, 30 min preincubation) to cause accumulation of this otherwise short-lived metabolic intermediate. AngII stimulation (60 min) increases incorporation into CDP-DAG from a very low resting level and this response is completely eliminated by the inhibition of DGKs but only partially impaired by treatment with the phospholipase C (PLC) inhibitor, U73122, and marginally affected by inhibition of PLD. Values (mean ± SEM) of duplicate determinations from three independent experiments.
- D, E Effects of knock-down of the CDS1; CDS2 or DGKε enzymes on the AngII-induced increase in the incorporation of either [³H]-cytidine (D) or myo-[³H]-inositol (E) labeling of HEK293-AT1 cells. Only the knock down of CDS2 enzyme caused a significant drop in the AngII-stimulated increases. (means ± SEM are shown from four independent experiments performed in duplicates, except for inositol labeling in the group of combined knock-down of CDS1/2 which was performed twice).

Data Information: Statistical differences from the AngII-treated control cells were calculated using Student t-test with Welsh correction.

2022), for all practical reasons we treated these measurements as reflections of PI(4,5)P₂ changes. These analyses showed that the PIP₂ in these cultured cells showed a variable side-chain profile, with the major species being 38:4 and 34:1, which corresponds to the general profile of their shared precursor, PI (Fig 6A). The only clear discrepancy observed relative to PI was the larger representation of the 34:1 species of PIP₂. Stimulation of the cells with AngII showed a rapid decrease in all side-chain variants of PIP₂, which was followed by a slow recovery (Fig 6B). To compare the relative recovery rates for each fatty acyl form of PIP₂ independent of their representation, they were all expressed as a percent of their initial values in Fig 6B. Strikingly, this comparison showed that the rates of resynthesis of the various side-chain variants were markedly different; with the fastest and most complete recovery being associated with the 38:4 species, while the slowest recovery was observed for the shortest and most saturated species, with the rest lying in between (Fig 6B). It is notable that this analysis identified a small amount of the 32:0 form of PIP₂, whereas this species was poorly represented in PI. Please note that the PI fatty acid profiles shown in Figs 1C and 6C were obtained from two different lipidomic service providers and at different time periods (see Methods).

Nir2 is not responsible for the fatty acid selectivity during PI(4,5)P₂ recycling

Fatty acid discrimination during the recycling of the hydrolytic products of PI(4,5)P₂ breakdown could occur at the step of non-vesicular PI or PA transfer between the PM and ER or at the level of PI or CDP-DAG synthesis within the ER. Based on their PI transfer activity *in vitro*, Class I PIPTs have been shown to deliver PI from the ER to be used by PI 4-kinases, including those found in the Golgi complex as well as the PM, and are assumed to supply PI to the PM (Ashlin *et al.*, 2021). However, using KO cells generated by CRISPR/Cas9 gene-editing, we could not substantiate a role for PIP α or PIP β in PI4P and PI(4,5)P₂ maintenance during AngII-induced PLC activation in our HEK293-AT1 cells as measured by BRET analysis (Fig EV4A–D). In contrast, in agreement with the conclusion of earlier studies, (Chang *et al.*, 2013; Kim *et al.*, 2013), Nir2 knock-out (KO) cells did show an impairment in PI4P and PIP₂ recovery after AngII stimulation (Fig EV3B–D). Lipidomic analysis revealed that

the fatty acid profile of the PIP₂ species in the Nir2 KO cells was similar to those of the parent HEK293-AT1 cells (Fig 6B and D) and that the rate of recovery following AngII stimulation was still fastest for the 38:4 species of PIP₂ (Fig 6B and D). These data suggest that Nir2 is important, but not the sole mechanism by which PI is replenished in the PM and that the fastest recovery of the 38:4 species during the PIP₂ recycling process is not dependent on Nir2.

Discussion

Eukaryotic cells maintain unique lipid compositions within distinct organelle membranes. Most cellular lipids are synthesized in the ER and reach their destination either through vesicular trafficking or with the help of specialized proteins via non-vesicular lipid transport (Wong *et al.*, 2018; Prinz *et al.*, 2020). Cells also display a spectacular diversity in the individual phospholipid constituents that comprise organelle membranes, with lipid species differing substantially in their fatty acid side-chain lengths and degree of saturation. It is not understood whether the distinctive fatty acid side-chain composition of specific phospholipid classes has any role in determining their abundance in specific organelles or for defining their metabolic fates during enzymatic conversions. While these questions have been approached experimentally over the years using diverse approaches and biological specimens, there are very few investigations that have taken advantage of modern lipidomic techniques and applied these approaches to intact cells to follow dynamic changes in the cellular lipid landscape.

In the present study, we attempted to understand how cells achieve and maintain the unique enrichment of the 1-stearoyl and 2-arachidonoyl fatty acid configuration of the essential structural phospholipid, PI. Importantly, PI and its phosphorylated PPIn derivatives have a central role in the integrated control of cellular lipid homeostasis, vesicular trafficking, and metabolism (Balla, 2013; Schink *et al.*, 2016). PI is synthesized in a stepwise fashion, consuming PA and CDP-DAG as metabolic intermediates, in membranes of the ER or within an ER-derived mobile membrane compartment (Kim *et al.*, 2011). While PA is the ultimate precursor of PI and the PPIn lipids, it also serves as an important metabolic hub for lipid synthesis or storage and can be produced from various

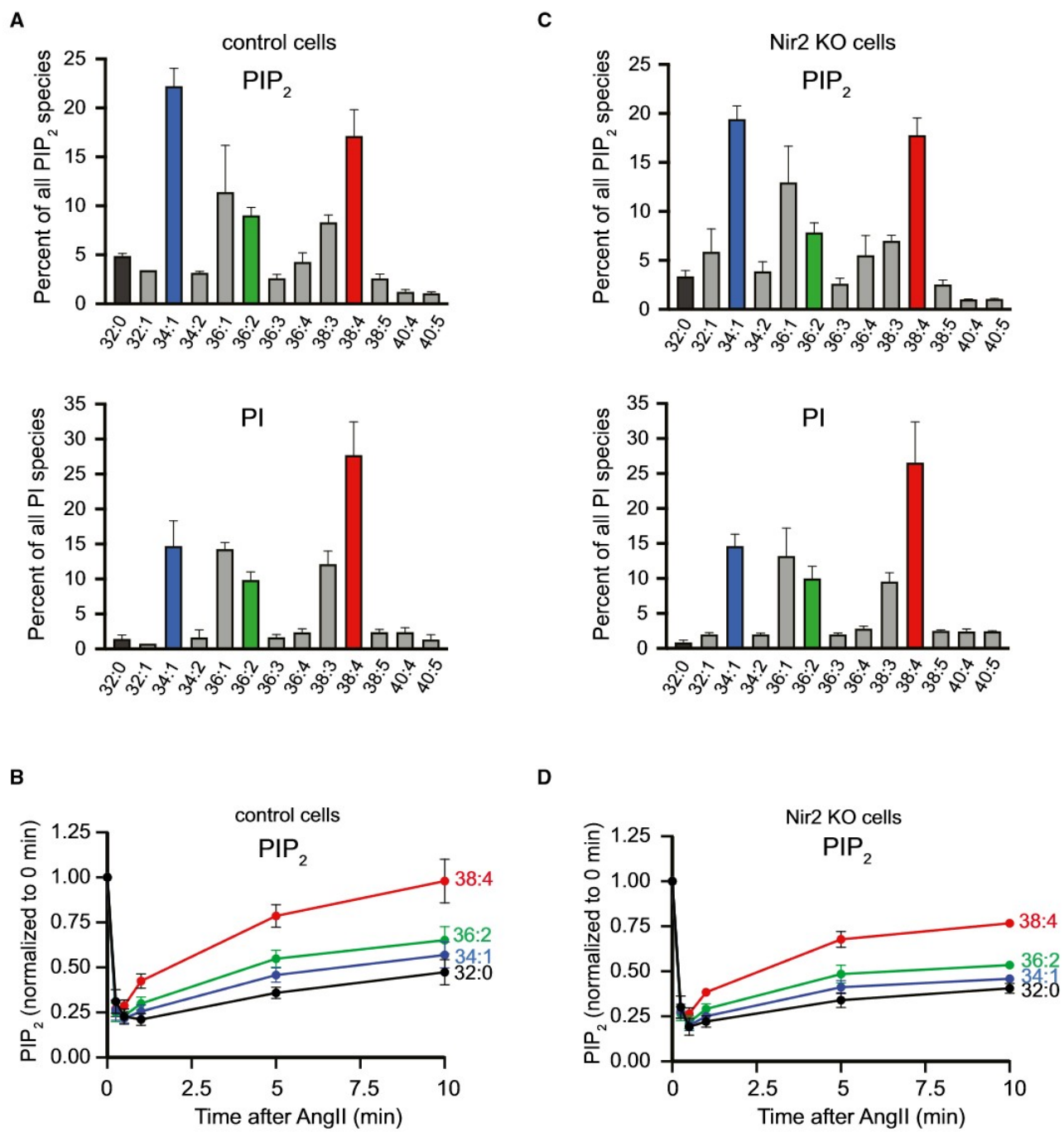


Figure 6. Changes in the various species of PIP₂ represented in HEK293-AT1 and Nir2 KO cells after stimulation with AngII.

(A–D) Relative abundance of the different species of phosphatidylinositol (PI) bisphosphate (PIP₂) and PI in HEK293-AT1 cells (A) and a Nir2 knockout (KO) cell line derived from them (C). Note the close correlation between the fatty acid side-chain profile of the PIP₂ and PI species, with the exception of the relatively larger fraction of the 34:1 species apparent in PIP₂ compared to PI. No major differences were observed between the wild-type and Nir2 KO cells. (B, D) Time course measurements monitoring changes in the various fatty acid side-chain variants of PIP₂ after stimulation with AngII. Note that the values are expressed as a percentage of each PIP₂ species at 0 min in order to accurately compare the kinetics of any changes observed. Also there is a difference in the speed of recovery between the various PIP₂ forms that is preserved in the Nir2 KO cells. Means \pm SD; $n = 3$ are shown for control cells; and means \pm range of $n = 2$ are shown for Nir2 KO cells from n independent experiments each performed in biological triplicates. The error bars in (C and D) correspond to the actual values of the two individual experiments.

sources. Briefly, PA is synthesized *de novo* from G3P, or generated from DAG by any of the many isoforms of DGK as well as produced by PLDs acting on PC (Fig 1A and B). Once synthesized, PA is not only the precursor for PI, but it can also be converted to DAG by the lipin phosphatases that can then feed into TG formation and lipid storage, or be used for the biosynthesis of other phospholipids; such as PC and PE via the Kennedy pathway (Fig 1B).

In this study, we found that in microsome membrane preparations, *de novo* synthesized PA was preferentially converted to TG, especially when oleoyl-CoA was used as a substrate. Saturated fatty acids, such as palmitoyl- or stearoyl-CoA were significantly poorer substrates for TG production, although palmitoyl-CoA was efficiently incorporated into PA. Conversion of PA to PI, however, was clearly favored when using the arachidonoyl-CoA substrate, even though it was not the preferred fatty acid for *de novo* PA synthesis. These important findings suggest that early steps in PA synthesis efficiently utilize palmitoyl-CoA, but that the PA to PI conversion is more favorable when arachidonoyl side chains are present. This conclusion was also supported by the results of lipidomic analyses showing that the major form of PA present in unstimulated cells was the dipalmitoyl 32:0 species, which was almost undetectable in PI. While the enrichment of the 38:4 configuration of PI via the Lands' cycle is well established and primarily mediated by the LPIAT1/MBOAT7 enzyme (Lee *et al.*, 2012; Anderson *et al.*, 2013), our results also suggest that side-chain selection takes place during PI synthesis from *de novo* synthesized PA. Moreover, the sensitivity of the process to the DGKi suggests that DAG serves as an intermediate even when PA is abundantly available. The fact that, compared to PA, the fatty acid profile of DAG included longer and more unsaturated species is also indicative that some fatty acid remodeling must take place at the level of DAG.

Early labeling studies using radioactive precursors, namely G3P, showed that the fatty acid profile of PA very closely matched that of the CDP-DAG product (Holub & Kuksis, 1971a; Holub & Piekarski, 1976; Nakagawa *et al.*, 1989). Since these analyses mostly relied upon the endogenous fatty acid supply in the preparation, the lipid composition was most likely determined by the available fatty acids and their preferential selection in the microsome preparations; as clearly shown in (Nakagawa *et al.*, 1989). Nevertheless, these studies did show that different forms of PA can be converted to CDP-DAG or PI and concluded that fatty acid remodeling is probably the result of deacylation–reacylation Land's cycles. Since these studies did not test various fatty acid analogues, they could not make conclusions regarding the relative side-chain preferences of these reactions. Importantly, the fatty acid composition of CDP-DAG from bovine brain was found to have the same high enrichment in the 1-stearoyl, 2-arachidonyl configuration as PI; arguing that this fatty acid preference occurs at least partially in the PA to CDP-DAG conversion step (Thompson & MacDonald, 1976). Relevant to these questions were more recent studies that compared relative substrate preference of the CDS enzymes for various species of PA using *in vitro* assays and found that CDS2, but not CDS1 or PIS, preferred 1-stearoyl, 2-arachidonoyl PA as a substrate (D'Souza *et al.*, 2014; D'Souza & Epand, 2015). Our knock-down studies also showed that the CDS2 enzyme plays a more important role in recycling the PLC hydrolytic products than the CDS1 enzyme. In fact, knock-down of CDS1 had no effect on isotope incorporation into PI or CDP-DAG whether knocked down alone or in combination with CDS2. We

attributed the partial effect of CDS2 knock-down on agonist-induced PI resynthesis to an incomplete knockdown of the protein.

The next question we asked was whether recycling of the lipid products generated during agonist stimulation showed some fatty acid preferences. First, we found that AngII stimulation yielded PA species that mostly followed the fatty acid composition of PIP₂, the primary target of the activated PLC. The minor contribution of PLD-derived PA bore the fatty acid signature of the major PC species. The PA increases that were observed in the short and saturated forms, which are not represented in PIP₂, most likely derive from an increased *de novo* PA synthesis. Isotope labeling studies were subsequently used to complement the lipidomics data and evaluate the source of PA utilized for the increased PI synthesis during AngII stimulation. These studies showed that PLC activity is the major source of PA used for rapid PI re-synthesis, with PLDs making little contribution. Notably, we found a discrepancy between the isotope labeling experiments and the lipidomics studies regarding sensitivity to the DGKi. The agonist-induced increase in the labeling of both CDP-DG and PI was completely eliminated by R59022, but not the knock-down of DGKe. However, the lipidomics data and BRET measurements of PA increases within the PM suggest that R59022 did not fully eliminate the observed elevations in PA. This suggested that some DGKs were not inhibited equally by the inhibitor, which is supported by direct enzymatic assays examining the potency of R59022 towards the various isoforms of DGK (Sato *et al.*, 2013). Why the R59022-resistant increases in PA are not translated into [³H]-inositol- or [³H]-cytidine-labeled PI or CDP-DG products is still an open question that warrants further investigation.

Finally, analysis of the fatty acid profiles of PIP₂ during AngII stimulation after normalization to their relative pre-stimulatory abundance showed that the speed of re-synthesis for the 38:4 forms of PIP₂ was faster than those esterified with more saturated and shorter fatty acids. Since the different recovery rates of PIP₂ did not correlate with the relative abundance of the different fatty acyl species in either the larger PI pool or of the initial PIP₂ pools, we have to assume that the unsaturated lipid intermediates are more efficiently recycled back to the PM pool of PIP₂. This was consistent with the labeling studies and argued for preferential recycling of the unsaturated PI(4,5)P₂ hydrolytic products. One source of the selectivity can theoretically be in the transport step(s) that move PA from the PM to ER and/or PI from the ER into the PM. This possibility is quite attractive because PITPs can interact with the fatty acid side chains of the bound lipid cargoes within the lipid-binding cavity. While class I PITPs (PITP α and PITP β) have been assumed to play a role in the supply of PM with the ER-synthesized PI, our studies using KO cells could not substantiate such a role as judged by the recovery kinetics of PI4P or PI(4,5)P₂ in the PM. Since the multi-domain PITP protein, Nir2, was previously shown to play a role in PI and PA exchange at ER-PM contact sites (Chang *et al.*, 2013; Kim *et al.*, 2013, 2015; Chang & Liou, 2015), we explored the involvement of Nir2 using specific KO cell lines. In agreement with previous studies (Kim *et al.*, 2013; Chang & Liou, 2015), Nir2 inactivation was impaired, but did not abolish PI4P and PI(4,5)P₂ recovery during agonist stimulation. However, the relative speed of the recovery of the different PIP₂ species showed the same difference in control and Nir2 KO cells. These results argue against a central role of Nir2 in the faster recovery of the 38:4-enriched PIP₂ species, but they also do not rule out the possibility that other PI transfer

processes may play an important role in this process. Our studies could not establish a critical role for PIP α or PIP β in the process of PI4P and PI(4,5)P₂ resynthesis and highlight the possibility of substantial redundancy in the PI transfer processes used at the PM.

Neither the lipidomics nor isotope-labeling studies could provide information on the subcellular distribution of the various forms of the lipids followed in this study. It is safe to assume that most of the PIP₂ measured is found within the PM and that PLC acts primarily on this PM pool of PIP₂. It is also likely that the 32:0 and 34:1 species of PA are found predominantly in membranes of the ER. BRET measurements of the changes in PA and DAG using the Spo20 and PKDC1ab domains, respectively, as reporters gave us an idea about the kinetic changes in these lipids within the PM. One caveat in the use of these biosensors is that they may not respond equally to the various side-chain variants of the lipids they are designed to follow (Kassas *et al.*, 2012). Still, comparing the kinetics of the changes measured using BRET with those of the lipidomics, we could conclude that the primary DAG species produced within the PM are likely derived from the 38:4 and 34:1 variants of PI(4,5)P₂, while the short-chain versions of DAG are most likely to represent an ER-localized pool. It is also evident that PA shows a continuous accumulation in the PM while PI is reduced. Given the minor contribution of the PM to the overall PI pool present within cells (Pemberton *et al.*, 2020; Zewe *et al.*, 2020), the decrease in PI is likely to occur in the ER or other internal membranes. This then suggests that there is a bottleneck in some of the steps by which PA present in the PM can reach the ER and be recycled back to PI. Whether PA generated from the direct transport of DAG from the PM to the ER, as suggested from studies of E-Syt1 (Saheki *et al.*, 2016), contributes to the PI-cycle under the condition of agonist stimulation remains an open question.

In summary, our studies indicate that the 1-stearoyl, 2-arachidonoyl enrichment of PI and its derivatives are established and maintained at multiple levels, even under strong agonist stimulation. While deacylation–reacylation of PI is a primary source of such enrichment, part of the fatty acid selectivity also occurs at the level of CDP-DAG production from PA within the ER. Equally important, our studies show a clear preference for the recycling of the PLC-produced lipid metabolites of PIP₂ hydrolysis; especially the 38:4 species. These studies suggest metabolic channeling of different sources of PA in the ER, with the preferred route of the *de novo* synthesized PA being directed toward forming TG for lipid storage, whereas PLC-mediated PA generation is preferentially used for PI synthesis; primarily by the CDS2 enzyme. These processes appear to ensure that the unique fatty acid composition of PI is maintained upon receptor stimulation. Overall, these studies detailing the regulatory mechanisms that contribute to the unique metabolic turnover of PI will serve as the foundation for future studies that can address the biological significance of the special fatty acid signature of PI and its essential PPIN derivatives.

Materials and Methods

Materials

Angiotensin II (human octapeptide) and DAG kinase inhibitor I (R59022) were from Bachem (Vista, CA) and Calbiochem

(Burlington MA), respectively. U73122, CTP, Inositol, CDP-choline, and all Acyl-CoA substrates were purchased from Sigma Aldrich (St Louis, MO). Coelenterazine h (1-361301-200) was purchased from Regis Technologies (Morton Grove, IL) and dissolved in 100% ethanol (vol/vol). The Nir2 antibody was raised against the peptide CRSRGPSQAEREGPG in rabbits and affinity purified (New England Peptide). The polyclonal rabbit anti-PIP α ("103") and monoclonal anti-PIP β ("1C1") antibodies were kind gifts of Dr. Shamshad Cockcroft (University College, London, UK). The monoclonal Tubulin antibody (clone Tub 2.1) was from Sigma.

DNA constructs and siRNAs

pET-28b(+)Lipin1 γ (isoform 4) (Han & Carman, 2010) was kindly provided by Dr. George Carman (Rutgers Center for Lipid Research, NJ) and subcloned into GFPNI plasmid using Xhol and NheI restriction sites. The single plasmid-based BRET constructs to follow DAG and PA changes in the PM have been described previously (Pemberton *et al.*, 2020). siRNA-SMARTpools for human PIP α (gene id:5306); PIP β (gene id:23760); CDS1 (gene id: 1040); CDS2 (gene id: 8760) and DGK ϵ (gene id: 8526) were purchased from GE Dharmacon/Horizon Discovery. AllStars Negative control siRNA was obtained from Qiagen.

Cell culture and transfections

HEK293-AT1 cells, which stably express the rat AT1a AngII receptor (Hunyady *et al.*, 2002), were cultured in DMEM with high glucose and sodium pyruvate (GIBCO) containing 10% FBS (GE Hyclone) and supplemented with a 1% solution of penicillin/streptomycin (GIBCO). The cell line has been regularly tested for Mycoplasma contamination using mycoplasma detection kit ("MycoAlert™ Mycoplasma Detection kit" from Lonza) and treated with Plasmocin prophylactic (InvivoGen, San Diego, CA) at 25 μ g/ml for 1 week after thawing. The subsequent passages were maintained at 5 μ g/ml of the Plasmocin prophylactic.

For BRET measurements, HEK293-AT1 cells were plated onto white 96-well plates that were precoated with 1:100 dilution of poly-L-lysine (Sigma). 40,000 cells/well were plated for DNA transfection and 20,000 cells/well for experiments involving 3 days of siRNA treatment. Cells were transfected with 0.1 μ g/well plasmid DNA using Lipofectamine 2000 reagent or 100 nM of siRNA using RNAiMax according to the manufacturer's instructions (Thermo Fisher Scientific). Cells were subjected to BRET analysis after 25–27 h transfection with BRET probes, while siRNA treatment was started 2 days prior to transfection of the BRET sensors.

Production of PIP α KO cells with CRISPR/Cas9 system

For each of the PIP α proteins (Nir2, PIP α and PIP β), three targeting sequences were designed with Optimized CRISPOR Design (<http://crispor.tefor.net>) targeting specific exon sequences (exon 2 for Nir2/PITPNM1 and PIP β /PITPNB and exon 4 for PIP α /PITPNA) in the human genome. The target sequences were ordered as oligonucleotide pairs and were inserted into a modified plenti-CRISPR v2 plasmid (Jones *et al.*, 2017) using a BsmBI site. This plasmid was used straight (not in the form of a virus) for transfection followed by puromycin (5 μ g/ml) selection for 3 days. Gene editing

efficiency of the three gRNAs was tested with T7 Endonuclease I (New England Biolab) digestion of PCR fragments covering the target sequence, and the best gRNAs were chosen to create KO cells: (PITPNM1: 5'-ACGGATGGGCCGGGGCAG-3'; PITPNB: 5'-CCTGCCTGTGTCAGATG-3'; PITPNB: 5'-CTCACCTCCTGAACAGAAC-3'). HEK293-AT1 cells (500,000 cells/well) were seeded into a 6 well plate and transfected with 8 µg of the target plasmid the next day using Lipofectamine LTX. After incubation overnight, the cells were cultured with 5 µg/ml puromycin in the media for 3 days. The cells were grown without puromycin for a few more days before splitting at a density to achieve a single cell per well in 96 well plates. Single colonies from the 96 wells were transferred and grown in 6 well plates. Individual clones were then screened with Western blotting analysis using the respective anti-PITP antibodies. Several clones were then subjected to lipidomics and confocal microscopy.

BRET measurement

After 25–27 h of transfection, HEK293-AT1 cells were rinsed with modified Krebs–Ringer buffer (containing 120 mM NaCl, 4.7 mM KCl, 2 mM CaCl₂, 0.7 mM MgSO₄, 10 mM glucose, and 10 mM Hepes, adjusted to pH 7.4) and incubated in 50 µl/well Krebs–Ringer buffer for 30 min at 37°C before measurements. BRET measurements were carried out at 37°C using a Tristar2 LB 942 Multimode Microplate Reader (Berthold Technologies) with customized emission filters (485 and 530 nm). After the 30-min preincubation period, the cell-permeable luciferase substrate, coelenterazine h (40 µl diluted in the Krebs–Ringer solution to achieve a final concentration of 5 µM), was added, and the signal from the mVenus fluorescence and Luciferase luminescence were recorded using the 485- and 530-nm emission filters over a 4-min period of baseline BRET measurement. Following the baseline recordings, various treatments dissolved in the modified Krebs–Ringer solution, were added in 10 µl volume using a repeater pipet to achieve good mixing. Measurements were then continued for the indicated times. All measurements were performed in triplicate wells. BRET ratios (mVenus/Luciferase) were calculated for each well by dividing the 530-nm with the 485-nm intensity values.

Lipidomics analyses

HEK293-AT1 cells (600,000 cells/well, passage 6–9) were plated onto 60 mm culture dishes and cultured for 2 days. Individual inhibitors were added for 10 min prior to AngII stimulation in DMEM with high glucose medium and without serum. For analysis of phospholipids and DAG, reactions were terminated by removing the medium quickly and adding 1 ml of ice-cold 5% perchloric acid (PCA). After incubation on ice for 10 min, cells were frozen at –80° C. After thawing, cells were scraped in the 5% PCA solution, transferred to polypropylene tubes (ultrahydrophobic DNA Lo-Bind tubes from Eppendorf were used) and an additional wash of 400 µl of 5% PCA was combined in the same tubes. Samples were centrifuged at 18,000 g for 10 min and the PCA solution was removed from the cell pellet. Cell pellets were then sonicated in the 300 µl of PBS (at 6,000 cells/µl) and frozen on dry ice for shipment to Lipotype GmbH (Dresden, Germany) for analysis. For PPI_n (PI, PIP, and PIP₂) analysis, reactions were terminated with 0.5 M trichloroacetic acid (TCA) instead of PCA on ice. Cells were scraped and transferred into the polypropylene tubes and centrifuged at 20,000 g for 3 min. Pellets were gently washed with 5% TCA and 10 mM EDTA and re-centrifuged. After removing the medium, cell pellets were frozen and shipped on dry ice to ATK Analytics and Discovery (Seattle, Washington, USA), where the analysis was performed.

acid (TCA) instead of PCA on ice. Cells were scraped and transferred into the polypropylene tubes and centrifuged at 20,000 g for 3 min. Pellets were gently washed with 5% TCA and 10 mM EDTA and re-centrifuged. After removing the medium, cell pellets were frozen and shipped on dry ice to ATK Analytics and Discovery (Seattle, Washington, USA), where the analysis was performed.

In vitro GPAT assays

HEK293-AT1 cells (5,000,000 cells/dish) were cultured for two days in 100 mm culture dishes. For expression of Lipin 1γ, cells were transfected with 1 µg/dish plasmid DNA coding for GFP-Lipin1γ using Lipofectamine 2000 reagents. Cells were scraped and homogenized in 2 ml ice-cold buffer (250 mM sucrose, 10 mM Tris, pH 7.5, 1 mM EDTA, 1 mM dithiothreitol) with 10 times trituration up-and-down through a 25G syringe needle. Cell homogenates were then centrifuged briefly at 600 g for 5 min to remove nuclei and cell debris. The post nuclear fraction was then centrifuged at 10,000 g for 10 min to remove mitochondria. The post-mitochondrial membrane was collected by centrifugation at 100,000 g for 1 h to obtain the microsome pellet. Microsomes were resuspended in 200 µl buffer (50 mM Tris pH 8, 100 mM KCl, 0.1 mM EDTA, 0.1 mM dithiothreitol, 1 mM sodium fluoride and protease inhibitors). Lipid synthesis was assayed for 30 min at room temperature in a 100-µl reaction mixture containing 100 mM Tris-HCl, pH 7.5, 4 mM MgCl₂, 1 mg/ml BSA (essentially fatty acid-free), 1 mM dithiothreitol, 1 mM NaF, 66 µM (1 µCi/reaction, 66 µM final) [¹⁴C]-glycerol 3-phosphate (ARC Radiolabeled Chemicals), and 10 µM final concentration of the various fatty acyl-CoA substrates (Chen *et al.*, 2008). The reaction was initiated by adding 10–15 µg of membrane protein in the presence or absence of 1 mM CTP, 10 µM myo-inositol or 0.5 mM CDP-choline. When the DGK inhibitor was used, it was added to the membrane preparation and incubated in the reaction buffer at room temperature for 15 min, before adding the fatty acyl-CoA substrate to start the reaction. The reaction was stopped with 350 µl of ice-cold methanol: chloroform (2:1, vol:vol). 125 µl of chloroform and 125 µl of H₂O were then sequentially added for phase separation and the samples were vigorously vortexed. After centrifugation at 1,000 g for 5 min, the lower phase was taken, dried under N₂ and dissolved in 100 µl of chloroform: methanol (9:1; vol:vol) for application to silica gel 60 TLC plates (Merck, Millipore, Sigma). TLC plates were developed with a solvent system of [chloroform: methanol: H₂O; 65:25:4 (vol:vol:vol)] and subjected to autoradiography followed by phosphorimaging for quantification. In some cases the radioactivity was measured by a TLC scanning device RITA (RayTest, Germany).

In vitro PIS and CDS assays

Crude membranes were prepared from COS-7 cells transfected with plasmid DNAs coding for the respective enzymes (PIS-GFP or Myc-CDS2) as described previously (Kim *et al.*, 2011). For the PIS assay the reaction mixture contained 50 mM Tris-HCl pH 8.0, 100 mM KCl, 20 mM MgCl₂, 0.15% Triton X-100, 2 mM MnCl₂, 5 µCi myo-[³H]-inositol, 0.05 mM myo-inositol, 0.2 mM CDP-DAG (Avanti Polar lipids) and an aliquot of the crude membrane, all in a total volume of 0.1 ml.

After 30 min incubation at 37°C, the reaction was stopped by adding 0.35 ml of acidic methanol (0.1N HCl), followed by 0.5 ml of chloroform and 0.5 ml of 1 M MgCl₂. After vortexing, two phases were separated by centrifugation at 1,000 g for 2 min. The lower phase containing the chloroform fraction was transferred to scintillation vials, dried, and counted for radioactivity to determine the incorporation of *myo*-[³H]-inositol into PtdIns. In some cases, the inositol exchange reaction was monitored using *myo*-[³H]inositol, 0.2 mM PI and 0.1 mM CMP in the assay buffer. We found no difference between inhibitor sensitivities whether running the forward or exchange reactions.

For the CDS assays, PA (Egg, Chicken, Avanti Polar lipids) was dried under N₂, and resuspended in the assay buffer [50 mM Tris-HCl (pH 8.0), 100mM KCl, 2 mg/ml fatty acid free BSA] at a concentration of 1 mM and bath-sonicated for 30 sec. MgCl₂ was prepared in assay buffer at 40 mM concentration and mixed with the sonicated PA solution (1:1) giving a final concentration of PA and MgCl₂ at 0.5 mM and 20 mM, respectively. The microsomal membranes from COS-7 cells expressing myc-tagged CDS2 (30 µg protein) were incubated with 50 µM DAG kinase inhibitor in 0.1 ml reaction buffer for 10 min and the enzyme reaction was started by addition of 2.5 µCi CTP (cytidine 5'-[5'-³H]-triphosphate, 1mCi/ml, S.A. 20 Ci/mmol, ARC Radiolabeled Chemicals) and 0.2 mM CTP for 30 min at 37°C. The reaction was stopped by adding 500 µL of acidic methanol and followed by the addition of 300 µl of 0.6N HCl and 1 ml of chloroform. After vigorous vortexing, the solution was centrifuged at 1,000 g for 2 min and the upper phase was removed by suction and the lower organic phase was washed with 1 ml of ice-cold "upper phase" solution obtained from a mixture of methanol / 0.6N HCl/ chloroform [10:6:20 (vol:vol:vol)]. After centrifugation at 1,000 g for 2 min, the lower phase was transferred to scintillation vials, dried, and counted for radioactivity.

Analysis of *myo*-[³H]-inositol- or [³H]-cytidine-Labeled Lipids

HEK293-AT1 cells were plated on 12-well plates and cultured for 24 h. All inhibitors were added 10 min before the addition of the respective radioactive isotope. For *myo*-[³H]-inositol labeling the radioactive tracer (10 µCi/ml, S.A: 98 Ci/mmol, Perkin-Elmer) was added for 1hr in inositol-free DMEM supplemented with 50 µM unlabeled *myo*-inositol with or without AngII (100 n M). For [³H]-cytidine labeling, cells were incubated in inositol-free DMEM medium overnight in the presence of 2.5% dialyzed serum and labeled with 10 µCi/ml [³H]-cytidine (ARC Radiolabeled Chemicals) in a modified Krebs–Ringer solution for a total of 2 hr. LiCl (10 mM) was added 30 min after [³H]-cytidine followed 30 min later by AngII for an additional 60 min. Inhibitors were added 15 min before AngII. Reactions were terminated by the addition of ice-cold perchloric acid (to a final concentration of 5%), and cells were kept on ice for 30 min. After scraping and freeze-thawing, cells were centrifuged and the cell pellet was processed to extract lipids by an acidic chloroform/methanol extraction followed by TLC essentially as described previously (Nakanishi *et al*, 1995). For some experiments of [³H]-inositol- and [³H]-cytidine labeling, TLC was not performed but the entire extract was evaporated and analyzed by scintillation counting since a negligible amount of radioactivity was associated with lipids other

than PI and CDP-DG, respectively (Kim *et al*, 2015). When labeling experiments were done following RNAi treatment, HEK293-AT1 cells were seeded onto poly-L-lysine-coated 12 well tissue culture plates and transfected with the respective siRNAs (100 nM) for 3 days before labeling.

Quantitative real-time PCR analysis

HEK293-AT1cells were seeded onto poly-L-lysine-coated 12 well tissue culture plates and transfected with the 100 nM of the respective siRNA. After 3days total RNA was extracted using the RNAeasy mini kit from Qiagen. cDNA was synthesized using 4µg of RNA and the Omniscript RT kit (Qiagen) for each sample. Quantitative real-time PCR (qPCR) was performed using StepOne-Plus Real-Time PCR System, Taqman Universal PCR Master Mix and the Taqman gene expression assay (all from ThermoFisher scientific). Assay ID for each gene: CDS1(Hs00181633_m1), CDS2 (Hs00300881_m1), and DGKE (Hs01098268_g1). Expression levels were normalized to Human GAPDH (Hs02758991_g1) and data were analyzed using the ddCt method. All qPCR analyses were performed in triplicates.

Data availability

There are no data deposited in a public database.

Expanded View for this article is available online.

Acknowledgements

We would like to thank Drs. George Carman (Rutgers University, NJ) and Nicolas Vitale (University of Strasbourg, France) for DNA constructs as well as Dr. Shamsad Cockcroft (University College, London, UK) for the PITP antibodies. The generous help with the isotope scanning of TLC plates by the Prinz laboratory (NIDDK, NIH) is highly appreciated. This research was supported by the Intramural Research Program of the Eunice Kennedy Shriver National Institute of Child Health and Human Development of the National Institutes of Health and a Natural Sciences and Engineering Research Council of Canada (NSERC) Banting Postdoctoral Fellowship to JGP.

Author contributions

Yeon Ju Kim: Conceptualization; Formal analysis; Investigation; Methodology; Writing—review & editing. **Nivedita Sengupta:** Formal analysis; Methodology. **Mira Sohn:** Formal analysis; Methodology. **Amrita Mandal:** Data curation; Formal analysis; Methodology. **Joshua G Pemberton:** Conceptualization; Formal analysis; Methodology; Writing—review & editing. **Uimook Choi:** Resources; Methodology. **Tamas Balla:** Conceptualization; Data curation; Supervision; Funding acquisition; Investigation; Methodology; Writing—original draft; Project administration.

Disclosure of competing interest statement

The authors declare that they have nothing to disclose and have no conflict of interest related to this work.

Note added in proof

A parallel study investigating the mechanisms contributing to the unique fatty acid side-chain composition of phosphoinositides using different approaches has been published in The EMBO Journal (Barneda *et al*, 2022).

References

- Agranoff BW, Bradley RM, Brady RO (1958) The enzymatic synthesis of inositol phosphatide. *J Biol Chem* 233: 1077–1083
- Anderson KE, Juvín V, Clark J, Stephens LR, Hawkins PT (2016) Investigating the effect of arachidonate supplementation on the phosphoinositide content of MCF10a breast epithelial cells. *Adv Biol Regul* 62: 18–24
- Anderson KE, Kielkowska A, Durrant TN, Juvín V, Clark J, Stephens LR, Hawkins PT (2013) Lysophosphatidylinositol-acyltransferase-1 (LPIAT1) is required to maintain physiological levels of PtdIns and PtdInsP(2) in the mouse. *PLoS One* 8: e58425
- Ashlin TG, Blunsom NJ, Cockcroft S (2021) Courier service for phosphatidylinositol: PITPs deliver on demand. *Biochim Biophys Acta Mol Cell Biol Lipids* 1866: 158985
- Balla A, Kim YJ, Varnai P, Szentpetery Z, Knight Z, Shokat KM, Balla T (2007) Maintenance of hormone-sensitive phosphoinositide pools in the plasma membrane requires phosphatidylinositol 4-kinase III α . *Mol Biol Cell* 19: 711–721
- Balla T (2013) Phosphoinositides: tiny lipids with giant impact on cell regulation. *Physiol Rev* 93: 1019–1137
- Barameda D, Cosulich S, Stephens L, Hawkins P (2019) How is the acyl chain composition of phosphoinositides created and does it matter? *Biochem Soc Trans* 47: 1291–1305
- Barameda D, Janardan V, Niewczas I, Collins DM, Cosulich S, Clark J, Stephens LR, Hawkins PT (2022) Acyl chain selection in the synthesis of phosphoinositides. *EMBO J*. In Press
- Berger A, German JB (1990) Phospholipid fatty acid composition of various mouse tissues after feeding alpha-linolenate (18:3n-3) or eicosatrienoate (20:3n-3). *Lipids* 25: 473–480
- Berridge MJ (1984) Inositol trisphosphate and diacylglycerol as intracellular messengers. *Bio Chem J* 220: 345–360
- Bone LN, Dayam RM, Lee M, Kono N, Fairn GD, Arai H, Botelho RJ, Antonescu CN (2017) The acyltransferase LYCAT controls specific phosphoinositides and related membrane traffic. *Mol Biol Cell* 28: 161–172
- Chang CL, Hsieh TS, Yang TT, Rothberg KG, Azizoglu DB, Volk E, Liao JC, Liou J (2013) Feedback regulation of receptor-induced Ca²⁺ signaling mediated by e-syt1 and nir2 at endoplasmic reticulum-plasma membrane junctions. *Cell Rep* 5: 813–825
- Chang CL, Liou J (2015) Phosphatidylinositol 4,5-bisphosphate homeostasis regulated by Nir2 and Nir3 proteins at endoplasmic reticulum-plasma membrane junctions. *J Biol Chem* 290: 14289–14301
- Chen YQ, Kuo M-S, Li S, Bui HH, Peake DA, Sanders PE, Thibodeaux S J, Chu S, Qian Y-W, Zhao Y et al (2008) AGPAT6 is a novel microsomal glycerol-3-phosphate acyltransferase. *J Biol Chem* 283: 10048–10057
- Chang CL, Liou J (2016) Homeostatic regulation of the PI(4,5)P2-Ca²⁺ signaling system at ER-PM junctions. *Biochim Biophys Acta* 1861: 862–873
- D'Souza K, Epand RM (2015) The phosphatidylinositol synthase-catalyzed formation of phosphatidylinositol does not exhibit acyl chain specificity. *Biochemistry* 54: 1151–1153
- D'Souza K, Kim YJ, Balla T, Epand RM (2014) Distinct properties of the two isoforms of CDP-diacylglycerol synthase. *Biochemistry* 53: 7358–7367
- Epand RM (2012) Recognition of polyunsaturated acyl chains by enzymes acting on membrane lipids. *Biochim Biophys Acta* 1818: 957–962
- Gulyas G, Sohn M, Kim YJ, Varnai P, Balla T (2020) ORP3 phosphorylation regulates phosphatidylinositol 4-phosphate and Ca²⁺ dynamics at PM-ER contact sites. *J Cell Sci* 133: jcs237388
- Han GS, Carman GM (2010) Characterization of the human LPIN1-encoded phosphatidate phosphatase isoforms. *J Biol Chem* 285: 14628–14638
- Hasegawa J, Strunk BS, Weisman LS (2017) PI5P and PI(3,5)P2: minor, but essential phosphoinositides. *Cell Struct Funct* 42: 49–60
- Hashidate-Yoshida T, Hayayama T, Hishikawa D, Morimoto R, Hamano F, Tokuoka SM, Eto M, Tamura-Nakano M, Yanobu-Takanashi R, Mukumoto Y et al (2015) Fatty acid remodeling by LPCAT3 enriches arachidonate in phospholipid membranes and regulates triglyceride transport. *eLife* 4: e06328
- Hill EE, Lands WE (1968) Incorporation of long-chain and polyunsaturated acids into phosphatidate and phosphatidylcholine. *Biochim Biophys Acta* 152: 645–648
- Holub BJ (1975) Role of cytidine triphosphate and cytidine diphosphate in promoting inositol entry into microsomal phosphatidylinositol. *Lipids* 10: 483–490
- Holub BJ, Kuksis A (1971a) Differential distribution of orthophosphate-32 P and glycerol-14 C among molecular species of phosphatidylinositol of rat liver *in vivo*. *J Lipid Res* 12: 699–705
- Holub BJ, Kuksis A (1971b) Structural and metabolic interrelationships among glycerophosphatides of rat liver *in vivo*. *Can J Biochem* 49: 1347–1356
- Holub BJ, Pieckarski J (1976) Biosynthesis of molecular species of CDP-diglyceride from endogenously-labeled phosphatidate in rat liver microsomes. *Lipids* 11: 251–257
- Hunyady L, Baukal AJ, Gaborik Z, Olivares-Reyes JA, Bor M, Szaszak M, Lodge R, Catt KJ, Balla T (2002) Differential PI 3-kinase dependence of early and late phases of recycling of the internalized AT1 angiotensin receptor. *J Cell Biol* 157: 1211–1222
- Imae R, Inoue T, Nakasaki Y, Uchida Y, Ohba Y, Kono N, Nakanishi H, Sasaki T, Mitani S, Arai H (2012) LYCAT, a homologue of *C. elegans* acl-8, acl-9, and acl-10, determines the fatty acid composition of phosphatidylinositol in mice. *J Lipid Res* 53: 335–347
- Jones KR, Choi U, Gao J-L, Thompson RD, Rodman LE, Malech HL, Kang EM (2017) A novel method for screening adenosine receptor specific agonists for use in adenosine drug development. *Sci Rep* 7: 44816
- Kassas N, Tryoen-Toth P, Corrotte M, Thahouly T, Bader MF, Grant NJ, Vitale N (2012) Genetically encoded probes for phosphatidic acid. *Methods Cell Biol* 108: 445–459
- Kim S, Kedan A, Marom M, Gavert N, Keinan O, Selitrennik M, Laufman O, Lev S (2013) The phosphatidylinositol-transfer protein Nir2 binds phosphatidic acid and positively regulates phosphoinositide signalling. *EMBO Rep* 14: 891–899
- Kim YJ, Guzman-Hernandez ML, Balla T (2011) A highly dynamic ER-derived phosphatidylinositol-synthesizing organelle supplies phosphoinositides to cellular membranes. *Dev Cell* 21: 813–824
- Kim YJ, Guzman-Hernandez ML, Wisniewski E, Balla T (2015) Phosphatidylinositol-phosphatidic acid exchange by Nir2 at ER-PM contact sites maintains phosphoinositide signalling competence. *Dev Cell* 33: 549–561
- Koreh K, Monaco ME (1986) The relationship of hormone-sensitive and hormone-insensitive phosphatidylinositol to phosphatidylinositol 4,5-bisphosphate in the WRK-1 cell. *J Biol Chem* 261: 88–91
- Lee H-C, Inoue T, Sasaki J, Kubo T, Matsuda S, Nakasaki Y, Hattori M, Tanaka F, Udagawa O, Kono N et al (2012) LPIAT1 regulates arachidonic acid content in phosphatidylinositol and is required for cortical lamination in mice. *Mol Biol Cell* 23: 4689–4700
- Lykidis A, Jackson PD, Rock CO, Jackowski S (1997) The role of CDP-diacylglycerol synthetase and phosphatidylinositol synthase activity levels in the regulation of cellular phosphatidylinositol content. *J Biol Chem* 272: 33402–33409

- Malek M, Kielkowska A, Chessa T, Anderson KE, Barneda D, Pir P, Nakanishi H, Eguchi S, Koizumi A, Sasaki J et al (2017) PTEN regulates PI(3,4)P₂ signaling downstream of class I PI3K. *Mol Cell* 68: 566–580.e10
- Michell RH (1975) Inositol phospholipids and cell surface receptor function. *Biochim Biophys Acta* 415: 81–147
- Morioka S, Nakanishi H, Yamamoto T, Hasegawa J, Tokuda E, Hikita T, Sakihara T, Kugii Y, Oneyama C, Yamazaki M et al (2022) A mass spectrometric method for in-depth profiling of phosphoinositide regioisomers and their disease-associated regulation. *Nat Commun* 13: 83
- Nakagawa Y, Rustow B, Rabe H, Kunze D, Waku K (1989) The *de novo* synthesis of molecular species of phosphatidylinositol from endogenously labeled CDP diacylglycerol in alveolar macrophage microsomes. *Arch Biochem Biophys* 268: 559–566
- Nakanishi S, Catt KJ, Balla T (1995) A wortmannin-sensitive phosphatidylinositol 4-kinase that regulates hormone-sensitive pools of inositolphospholipids. *Proc Natl Acad Sci USA* 92: 5317–5321
- Nakano T, Matsui H, Tanaka T, Hozumi Y, Iseki K, Kawamae K, Goto K (2016) Arachidonoyl-specific diacylglycerol kinase epsilon and the endoplasmic reticulum. *Front Cell Dev Biol* 4: 132
- Pemberton JG, Kim YJ, Humpolickova J, Eisenreichova A, Sengupta N, Toth DJ, Boura E, Balla T (2020) Defining the subcellular distribution and metabolic channeling of phosphatidylinositol. *J Cell Biol* 219: e201906130
- Pettitt TR, Wakelam MJ (1999) Diacylglycerol kinase epsilon, but not zeta, selectively removes polyunsaturated diacylglycerol, inducing altered protein kinase C distribution *in vivo*. *J Biol Chem* 274: 36181–36186
- Poissmayer F, Scherphof GL, Dubbelman TM, van Golde LM, van Deenen LL (1969) Positional specificity of saturated and unsaturated fatty acids in phosphatidic acid from rat liver. *Biochim Biophys Acta* 176: 95–110
- Prinz WA, Toulmay A, Balla T (2020) The functional universe of membrane contact sites. *Nat Rev Mol Cell Biol* 21: 7–24
- Rodriguez de Turco EB, Tang W, Topham MK, Sakane F, Marcheselli VL, Chen C, Taketomi A, Prescott SM, Bazan NG (2001) Diacylglycerol kinase epsilon regulates seizure susceptibility and long-term potentiation through arachidonoyl- inositol lipid signaling. *Proc Natl Acad Sci USA* 98: 4740–4745
- Saheki Y, Bian X, Schauder CM, Sawaki Y, Surma MA, Klose C, Pincet F, Reinisch KM, De Camilli P (2016) Control of plasma membrane lipid homeostasis by the extended synaptotagmins. *Nat Cell Biol* 18: 504–515
- Saito S, Goto K, Tonosaki A, Kondo H (1997) Gene cloning and characterization of CDP-diacylglycerol synthase from rat brain. *J Biol Chem* 272: 9503–9509
- Sato M, Liu K, Sasaki S, Kunii N, Sakai H, Mizuno H, Saga H, Sakane F (2013) Evaluations of the selectivities of the diacylglycerol kinase inhibitors R59022 and R59949 among diacylglycerol kinase isozymes using a new non-radioactive assay method. *Pharmacology* 92: 99–107
- Schink KO, Tan KW, Stenmark H (2016) Phosphoinositides in control of membrane dynamics. *Annu Rev Cell Dev Biol* 32: 143–171
- Shulga YV, Anderson RA, Topham MK, Epand RM (2012) Phosphatidylinositol-4-phosphate 5-kinase isoforms exhibit acyl chain selectivity for both substrate and lipid activator. *J Biol Chem* 287: 35953–35963
- Sohn M, Korzeniowski M, Zewe JP, Wills RC, Hammond GRV, Humpolickova J, Vrzal L, Chalupska D, Veerka V, Fairn GD et al (2018) PI(4,5)P₂ controls plasma membrane PI4P and PS levels via ORP5/8 recruitment to ER-PM contact sites. *J Cell Biol* 217: 1797–1813
- Thompson W, MacDonald G (1976) Cytidine diphosphate diglyceride of bovine brain. Positional distribution of fatty acids and analysis of major molecular species. *Eur J Biochem* 65: 107–111
- Toth JT, Gulyas G, Hunyady L, Varnai P (2019) Development of nonspecific BRET-based biosensors to monitor plasma membrane inositol lipids in living cells. *Methods Mol Biol* 1949: 23–34
- Traynor-Kaplan A, Kruse M, Dickson EJ, Dai G, Vivas O, Yu H, Whittington D, Hille B (2017) Fatty-acyl chain profiles of cellular phosphoinositides. *Biochim Biophys Acta* 1862: 513–522
- Walther TC, Chung J, Farese Jr RV (2017) Lipid droplet biogenesis. *Annu Rev Cell Dev Biol* 33: 491–510
- Wong LH, Gatta AT, Levine TP (2018) Lipid transfer proteins: the lipid commute via shuttles, bridges and tubes. *Nat Rev Mol Cell Biol* 20: 85–101
- Zewe JP, Miller AM, Sangappa S, Wills RC, Goulden BD, Hammond GRV (2020) Probing the subcellular distribution of phosphatidylinositol reveals a surprising lack at the plasma membrane. *J Cell Biol* 219: e201906127